ELSEVIER

Spectrochimica Acta Part B 53 (1998) 1679–1703

SPECTROCHIMICA ACTA
PART B

Collisional–radiative model for the sputtered copper atoms and ions in a direct current argon glow discharge

Annemie Bogaerts[a,*], Renaat Gijbels[a], Robert J. Carman[b]

[a]*Department of Chemistry, University of Antwerp, Universiteitsplein 1, B-2610 Antwerp, Belgium*
[b]*Center for Lasers and Applications, Macquarie University, Sydney, Australia NSW 2109*

Received 21 July 1998; accepted 21 July 1998

Abstract

A collisional–radiative model is developed for various levels of the sputtered copper (Cu) atoms and their ions in an argon (Ar) direct current glow discharge, used as an analytical source for optical emission spectrometry. In this application, attention is paid to the photons emitted by sputtered atoms and ions, and hence to the behavior of excited levels of these species. 8 Cu atomic and 7 Cu^+ ionic levels are considered in the model, as well as the Cu^{2+} ions. Typical results of the model are the level populations (in two dimensions) of the various levels, and the relative contributions of the different populating and depopulating processes. This model is not only of interest for analytical glow discharge optical emission spectrometry, but also for plasma diagnostic tools and for copper–vapor lasers.

1. Introduction

In the last decades, glow discharges are finding increasing application in a number of fields, e.g., in the microelectronics industry (for etching of surfaces and for deposition of thin films), and as lasers, light sources and plasma display panels. Moreover, they are also being used as spectroscopic sources for elemental analytical chemistry [1, 2]. In the latter application, the cathode of the glow discharge is constructed from the material to be analyzed. Since the cathode is being sputtered by the plasma species (gas ions and fast atoms), the atoms of the cathode material (i.e., material to be analyzed) arrive in the plasma. Hence, the glow discharge plasma can be seen as an atom reservoir with a composition characteristic for the material to be analyzed. Atomic absorption or atomic fluorescence spectroscopy (GD-AAS and GD-AFS) can be applied to measure the atomic concentration in the plasma and hence in the material. On the other hand, the sputtered atoms are also subject to collisions in the plasma. They can be ionized, and the resulting ions can be detected in a mass spectrometer, which is exploited in glow discharge mass spectrometry (GDMS). Moreover, they can also be excited, and the characteristic photons emitted in the subsequent de-excitation can be probed by optical emission spectrometry (GD-OES).

Bogaerts et al. have developed a comprehensive set of models for an argon (Ar) glow discharge with copper (Cu) cathode, used in analytical chemistry (e.g., Refs. [3–10]). Special attention was being paid to the use of glow discharges for GDMS and hence to the ionization processes of the sputtered atoms and the behavior of the corresponding ions [8, 10]. In the present paper, however, we focus on the excitation of the sputtered atoms and their ions, and

* Corresponding author. Tel.: + 32-3820-2364; Fax: + 32-3820-2376; e-mail: bogaerts@uia.ua.ac.be.

0584-8547/98/$ - see front matter
PII: S0584-8547(98)00201-8

the population distributions over the various excited levels. This will make it possible later on to calculate the intensities of various spectral lines of the sputtered atoms and ions, which is of direct interest for GD-OES. Moreover, the present model can also be of interest for plasma diagnostic tools (intensities of spectral lines, e.g. for the determination of various kinds of temperatures in the plasma) and for copper vapor lasers.

The behavior of various excited levels is generally described in so-called collisional–radiative models (e.g., Refs. [11–14]), i.e., the population of the levels is determined by a number of collisional and radiative populating and depopulating processes. In a previous work, a collisional–radiative model has been developed for the Ar atoms in an Ar glow discharge, consisting of 65 effective levels (i.e., various levels were sometimes grouped together into one effective level) [14]. Excitation, de-excitation, ionization and recombination for all the levels, due to collisions with electrons, argon ions and atoms, were taken into account, as well as radiative decay between the levels, and some other collision processes for the Ar metastable levels (i.e., Penning ionization by sputtered atoms, metastable atom–metastable atom collisions, two-body and three-body collisions with argon ground state atoms, and diffusion and subsequent de-excitation at the walls) [14]. Cross sections and transition probabilities for all these processes are used as inputs in the model. Such data are, in general, much easier to find in the literature for Ar (and other gas) atoms than, for example, for Cu atoms. Therefore, most collisional–radiative models for glow discharges in the literature deal with gas atoms only (argon, helium, neon, …). However, some models have been developed for Cu as well, being applied to copper vapor lasers (e.g., Refs. [15–18]).

In this paper, a collisional–radiative model for copper atoms and ions will be presented. The levels taken into account are the same as in the models described in Refs. [16, 17]. However, the present model is applied to completely different conditions: i.e., a glow discharge used for GD-OES instead of a copper vapor laser, with argon as the discharge gas instead of neon, description of the cathode dark space and negative glow regions instead of the positive column. Moreover, some other modifications were carried out. Indeed, in the models of Refs. [16, 17] a two-electron group model (i.e., bulk and tail electrons), which incorporates a bi-Maxwellian electron energy distribution function, has been used to characterize the electron energies. This approximation is justified for the positive column of the copper vapor laser. However, the glow discharge under study here consists only of a cathode dark space and a negative glow, and it operates at high voltages (typically 1 kV). Hence, a strong electric field is present in the cathode dark space, and the electrons are not characterized by a Maxwellian distribution. Therefore, the electron behavior is simulated explicitly with a Monte Carlo method [3, 5, 9]. This method treats the electrons on the lowest microscopic scale. A large number of electrons are followed separately, one after the other, during successive time-steps. Their trajectory in the electric field is calculated by Newton's laws, and their collisions (the occurrence of a collision, and the new energy and direction after collision) are determined by random numbers, based on energy and angular differential cross sections. By following in this statistical way a large number of electrons, their behavior can be simulated explicitly, i.e., the exact energy gain from the electric field and energy loss due to collisions are calculated exactly instead of assuming a Maxwellian distribution.

Moreover, some other collisional processes, which were not incorporated in Refs. [16, 17] are now included in the model, like asymmetric charge transfer between argon ions and copper atoms. It was indeed demonstrated that this process is important at typical GD-OES discharge conditions [19]. Finally, the present model is developed in two dimensions and is applied to a cylindrically symmetrical discharge cell.

In Section 2, the model will be described in detail, and the input data (cross sections, transition probabilities, etc.) will be discussed. Section 3 will present typical calculation results, such as the level populations and the role of various populating and depopulating processes. Finally, the conclusion will be given in Section 4.

2. Description of the model

2.1. Model set-up

As mentioned above, our model deals with a glow

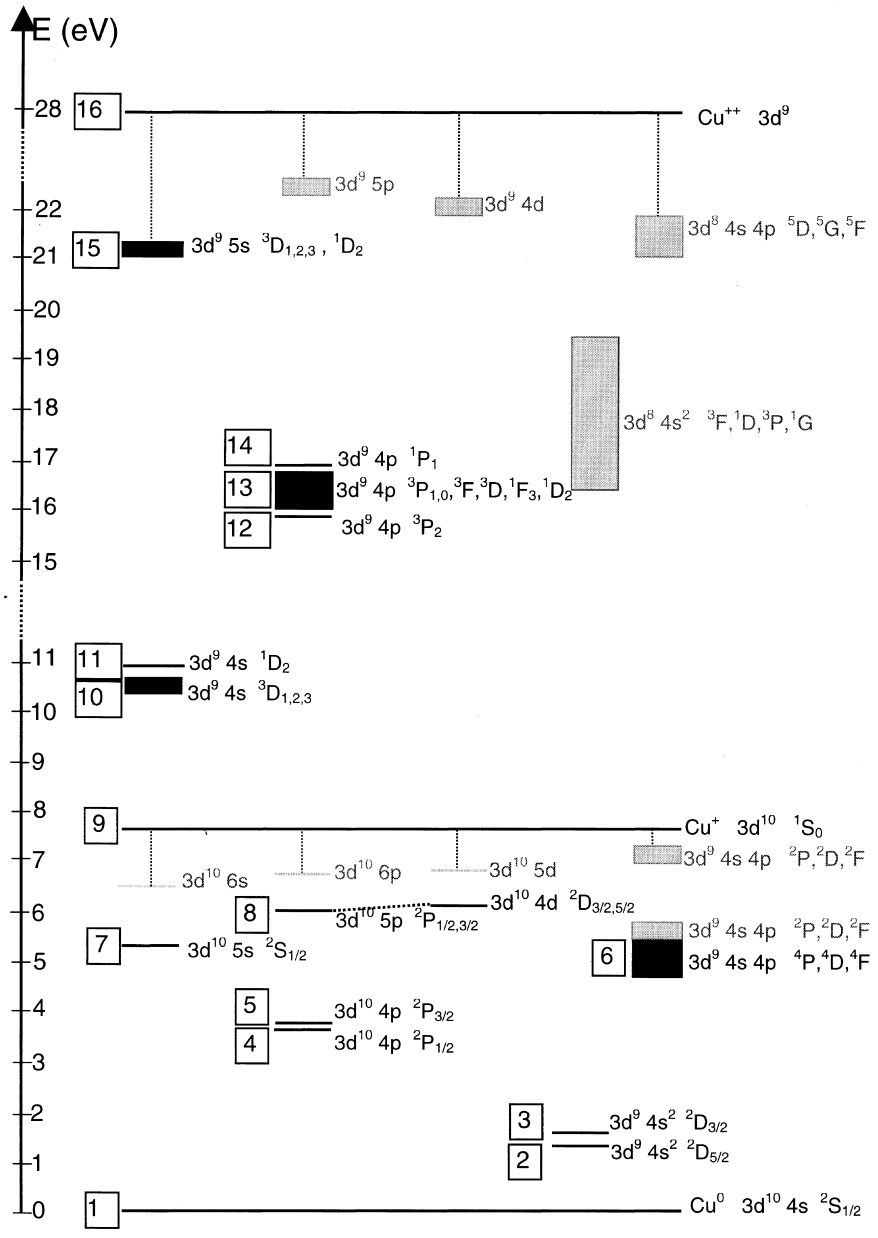

Fig. 1. Energy level scheme of the Cu atoms and ions, with the effective level number (left) and the designation according to Moore (right of the levels). The levels considered in the model are presented in black.

discharge consisting of a small cathode dark space adjacent to the cathode (characterized by a strong electric field), a negative glow region, which is nearly field-free and fills up the larger part of the discharge, and a small anode zone adjacent to the anode walls. Argon is assumed as the discharge gas, and the cathode material is made of pure copper. The species assumed to be present in the plasma, are argon gas atoms in thermal equilibrium (a gas temperature of 800 K is assumed at the discharge conditions under

Table 1
Effective level numbers (n) of the various levels incorporated in the model, together with their designation (according to Moore [22]), their energy (with respect to the Cu atom ground state) and their total statistical weight

Effective level	Designation	Energy (eV)	Statistical weight
1	Cu^0 $3d^{10}$ 4s ($^2S_{1/2}$)	0.0	2
2	Cu^0 $3d^9$ $4s^2$ ($^2D_{5/2}$)	1.39	6
3	Cu^0 $3d^9$ $4s^2$ ($^2D_{3/2}$)	1.64	4
4	Cu^0 $3d^{10}$ 4p ($^2P_{1/2}$)	3.79	2
5	Cu^0 $3d^{10}$ 4p ($^2P_{3/2}$)	3.82	4
6	Cu^0 $3d^{10}$ 4s 4p (^4P, ^4D, ^4F)	5.20	60
7	Cu^0 $3d^{10}$ 5s ($^2S_{1/2}$)	5.35	2
8	Cu^0 $3d^{10}$ 5p ($^2P_{1/2}$, $^2P_{3/2}$), $3d^{10}$ 4d ($^2D_{3/2}$, $^2D_{5/2}$)	6.17	16
9	Cu^+ $3d^{10}$ ($^1S_0$)	7.72	1
10	Cu^+ $3d^9$ 4s ($^3D_3$, $^3D_2$, $^3D_1$)	10.53	15
11	Cu^+ $3d^9$ 4s ($^1D_2$)	10.98	5
12	Cu^+ $3d^9$ 4p ($^3P_2$)	15.96	5
13	Cu^+ $3d^9$ 4p ($^3P_1$, $^3P_0$, $^3F_4$, $^3F_3$, $^3F_2$, $^3D_3$, $^3D_2$, $^3D_1$, $^1F_3$, $^1D_2$)	16.46	52
14	Cu^+ $3d^9$ 4p ($^1P_1$)	16.85	3
15	Cu^+ $3d^9$ 5s ($^3D_3$, $^3D_2$, $^3D_1$, $^1D_2$)	21.24	20
16	Cu^{2+}	28.01	

consideration: 500 Pa, 800 V, 28 mA, based on experimental observations of Ferreira et al. [20]), singly charged positive argon ions, fast argon atoms created in collisions with fast argon ions, argon atoms in various excited levels, sputtered cathode copper atoms and copper ions, in various excited levels, and electrons.

These species are described by a set of Monte Carlo models (for the species which are not in equilibrium with the electric field, i.e., fast electrons throughout the whole discharge, the thermalization of sputtered atoms after they leave the cathode, and argon ions, fast argon atoms and copper ions in the cathode dark space where a strong electric field is present) and fluid models for the other species (slow electrons, argon ions and copper ions in the negative glow, and the argon and copper atoms in various excited levels). All the models are coupled to each other due to the interaction processes between the species. Moreover, Poisson's equation is solved, to calculate the electric field distribution from the computed charged species densities. Hence, the model is self-consistent. All the sub-models for the different species are explained in detail in Refs. [3–10, 14].

Typical results of the models are densities, fluxes and energy distributions of the various species, the potential and electric field distribution, information about collision processes in the plasma and sputtering at the cathode. At the typical discharge conditions encountered in Grimm-type discharges (which are under consideration here), the electron density is in the order of 10^{14} cm^{-3} [21], whereas the mean electron energy is in the order of 0.5 eV. Nevertheless, electrons with all kinds of energies, up to the maximum possible value (i.e., the discharge voltage, in the order of 1 kV) are also present.

It should be mentioned that the general electrical characteristics of the discharge (i.e., electron energy distribution, current–voltage–pressure relations, electron density, etc.) are calculated to be the same for both the pure argon discharge (i.e., when no model for the sputtered atoms and ions is considered) and for the argon discharge with copper cathode. Indeed, the copper atoms and ions play only a minor role. As will be shown later (see Figs. 6 and 7 below), the copper atom and ion densities are in the order of 10^{14} and 10^{12} cm^{-3} at maximum, which is still clearly lower than the argon atom and ion densities (ca. 10^{16}–10^{17} and 10^{14} cm^{-3}, respectively [21]).

In the present paper, the sub-model for the sputtered copper atoms and ions in the various excited levels is described. Fig. 1 shows the energy level

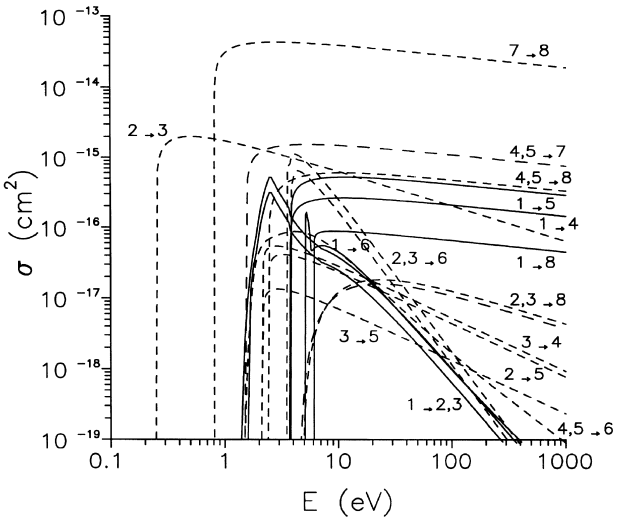

Fig. 2. Cross sections of electron impact excitation for the Cu atom levels, as a function of the electron energy. The cross sections for transitions from the ground state are indicated with solid lines, while the transitions between excited levels are presented with dashed lines.

scheme of the copper atoms and ions. Some of the levels, with energies lying close to each other, are grouped into an effective level. The levels taken into account in the model are presented with black lines. The other levels, which are shown in gray, were not incorporated, because cross sections for transitions from and to these levels are not known. However, the final goal of our work is to calculate spectral line intensities of copper atoms and ions, and those levels giving rise to the most intense spectral lines, are all included. The designation of the (effective) levels included in the model (according to Moore [22]), their energy (with respect to the Cu atom ground state) and statistical weight, are listed in Table 1. As can be seen, the $3d^9$ 4p Cu^+ ion levels are not all lumped together into one effective level. Indeed, the $3d^9$ 4p $^3P_2$ level is

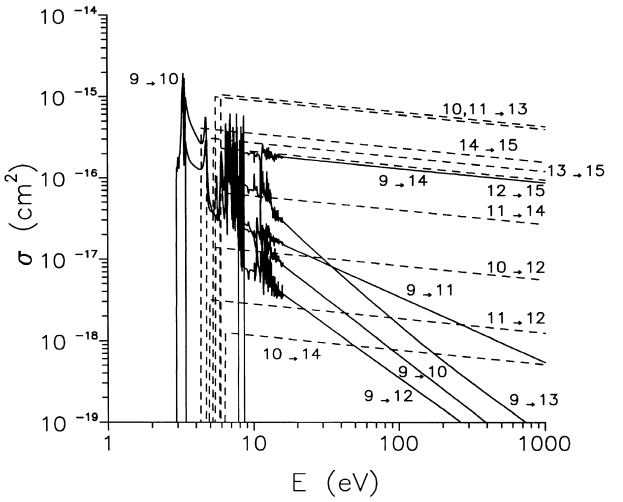

Fig. 3. Cross sections of electron impact excitation for the Cu^+ ion levels, as a function of the electron energy. The cross sections for transitions from the ground state are indicated with solid lines, while the transitions between excited levels are presented with dashed lines.

considered separately because it can be selectively excited by asymmetric charge transfer (see below and [19]). Similarly, the $3d^9\ 4p\ {}^1P_1$ level is also taken separately, because it is more efficiently excited by electron impact from the ground state (resonance transition) than the other $3d^9\ 4p$ levels (see Fig. 3). Beside the 8 Cu^0 atomic and the 7 Cu^+ ionic levels, also the Cu^{2+} ion (ground + excited levels together) is incorporated in the model.

The collisional and radiative processes taken into account in the model, are the following (grouped together with the inverse processes):

Electron impact excitation and de-excitation between the levels, for both Cu atoms and ions (n and m are arbitrary energy levels, with level m lying higher than level n):

$$\mathrm{Cu}(n) + \mathrm{e}^- \underset{R_{\mathrm{deexc,e}}}{\overset{R_{\mathrm{exc,e}}}{\rightleftarrows}} \mathrm{Cu}(m) + \mathrm{e}^-, \tag{1}$$

$$\mathrm{Cu}^+(n) + \mathrm{e}^- \underset{R_{\mathrm{deexc,e}}}{\overset{R_{\mathrm{exc,e}}}{\rightleftarrows}} \mathrm{Cu}^+(m) + \mathrm{e}^-. \tag{2}$$

Electron impact ionization; three-body recombination where the third body is an electron (i.e., transition from a Cu atom level to a Cu^+ ion level, and from a Cu^+ ion level to the Cu^{2+} ion, and vice versa).

$$\mathrm{Cu}(n) + \mathrm{e}^- \underset{R_{\mathrm{3b-recom}}}{\overset{R_{\mathrm{ionize,e}}}{\rightleftarrows}} \mathrm{Cu}^+(m) + \mathrm{e}^- + \mathrm{e}^-, \tag{3}$$

$$\mathrm{Cu}^+(n) + \mathrm{e}^- \underset{R_{\mathrm{3b-recom}}}{\overset{R_{\mathrm{ionize,e}}}{\rightleftarrows}} \mathrm{Cu}^{2+}(m) + \mathrm{e}^- + \mathrm{e}^-. \tag{4}$$

(Electron–ion radiative recombination could be neglected compared to three-body recombination, at the typical electron densities of $10^{14}\,\mathrm{cm}^{-3}$ encountered at the discharge conditions under investigation here.)

Electron impact ionization from the Cu atoms to the Cu^{2+} ions:

$$\mathrm{Cu}(n) + \mathrm{e}^- \overset{R_{\mathrm{ionize,e,2}}}{\longrightarrow} \mathrm{Cu}^{2+}(m) + \mathrm{e}^- + \mathrm{e}^- + \mathrm{e}^-. \tag{5}$$

Excitation and de-excitation between Cu atom levels, due to collisions with Ar gas atoms or Cu ground state atoms (since the Ar and Cu atoms have thermal energies, excitation will only occur between two closely lying levels; see further):

$$\mathrm{Cu}(n) + \mathrm{Cu}^0\ (\text{or } \mathrm{Ar}^0) \underset{R_{\mathrm{deexc,a}}}{\overset{R_{\mathrm{exc,a}}}{\rightleftarrows}} \mathrm{Cu}(m) + \mathrm{Cu}^0\ (\text{or } \mathrm{Ar}^0), \tag{6}$$

Penning ionization of Cu atoms, due to collisions with Ar metastable atoms:

$$\mathrm{Cu}(n) + \mathrm{Ar}_{\mathrm{m}}^* \overset{R_{\mathrm{PI}}}{\longrightarrow} \mathrm{Cu}^+(m) + \mathrm{Ar}^0 + \mathrm{e}^-. \tag{7}$$

Asymmetric charge transfer ionization of Cu atoms with Ar ions:

$$\mathrm{Cu}(n) + \mathrm{Ar}^+ \overset{R_{\mathrm{ACT}}}{\longrightarrow} \mathrm{Cu}^+(m) + \mathrm{Ar}^0, \tag{8}$$

Photo-excitation and radiative decay between all levels, for both Cu atoms and ions:

$$\mathrm{Cu}(n) + h\nu \underset{A(m,n)}{\overset{(1-\Lambda(m,n))\cdot A(m,n)}{\rightleftarrows}} \mathrm{Cu}(m), \tag{9}$$

$$\mathrm{Cu}^+(n) + h\nu \underset{A(m,n)}{\overset{(1-\Lambda(m,n))\cdot A(m,n)}{\rightleftarrows}} \mathrm{Cu}^+(m), \tag{10}$$

where $A(m,n)$ is the Einstein transition probability and $\Lambda(m,n)$ is the 'escape factor' (see below).

Further, the Cu atoms are created by sputtering at the cathode, and the transport of the Cu atoms and ions is described by diffusion for the atoms, and by diffusion and migration for the ions.

The level populations of the 8 Cu^0 atomic levels, the 7 Cu^+ ionic levels and the Cu^{2+} ground level are calculated with a set of 16 coupled balance equations (one for each level) describing all the different colli-

sional and radiative processes:

$$\frac{\partial N_n(z,r)}{\partial t} \bar{\nabla}\cdot\bar{J}_n(z,r) = R_{\text{prod}}(n)(z,r) - R_{\text{loss}}(n)(z,r), \tag{11}$$

where N_n is the population density of level n (for both the atomic and ionic levels), $\bar{J}_n$ is the particle flux (vector notation), and R_{prod} and R_{loss} comprise all production (populating) and loss (depopulating) processes of level n, respectively. All the variables are a function of z and r (i.e., axial and radial position), but in the following, these position coordinates are omitted, for the sake of simplicity.

For the atomic levels, production occurs by electron, Cu or Ar atom impact excitation from lower levels and de-excitation from higher levels, as well as radiative decay from higher levels. Moreover, the highest excited Cu atom level in the model can also be populated by three-body recombination between Cu ions and electrons. Finally, an additional production process is incorporated for the Cu ground state atoms, i.e., sputtering from the cathode. This leads to the following equation for atomic level n:

$$R_{\text{prod,atoms}}(n) = \sum_{l=1}^{n-1} \left[R_{\text{exc,e}}(l) + R_{\text{exc,a}}(l)\right] + \sum_{m=n+1}^{N_{\text{tot,at}}} \left[R_{\text{deexc,e}}(m) + R_{\text{deexc,a}}(m) + \Lambda(m,n)\cdot A(m,n)\right] + \sum_{i=1}^{N_{\text{tot,ion}}} \left[R_{\text{3b–recom}}(i)\right] + J_0 F_{\text{T}}, \tag{12}$$

where l and m denote the lower and higher atomic levels, respectively; i represents the ionic levels; and $N_{\text{tot,at}}$ and $N_{\text{tot,ion}}$ stand for the total number of atomic and ionic levels in the model. The third term is only used for the highest Cu atomic level ($n = 8$). The last term describes the production due to sputtering and is only used for the Cu atom ground state ($n = 1$). J_0 gives the flux of sputtered atoms from the cathode, and F_{T} symbolizes the three-dimensional thermalization profile of sputtered atoms, which is used as the starting distribution for diffusion (see below). The other symbols represent the rates of the various populating processes and were explained before in the process reactions.

The loss processes for the atoms include electron, Cu and Ar atom impact excitation to higher and de-excitation to lower levels, as well as radiative decay to lower levels. Also, ionization, given by electron impact ionization (both to Cu^+ and to Cu^{2+}), Penning ionization and asymmetric charge transfer, causes loss of the atomic levels:

$$\text{loss,atoms}(n) = \sum_{m=n+1}^{N_{\text{tot,at}}} \left[R_{\text{exc,e}}(m) + R_{\text{exc,a}}(m)\right] + \sum_{l=1}^{n-1} \left[R_{\text{deexc,e}}(l) + R_{\text{deexc,a}}(l) + \Lambda(n,l)\cdot A(n,l)\right] + R_{\text{ionize,e}}(\text{to } Cu^+) + R_{\text{ionize,e}}(\text{to } Cu^{2+}) + R_{\text{PI}} + R_{\text{ACT}}. \tag{13}$$

All the symbols are explained above. It should be mentioned that electron impact ionization to Cu^{2+}, Penning ionization and asymmetric charge transfer are only incorporated for the Cu atom ground state.

Finally, the transport by diffusion is expressed by:

$$\bar{J}_n(z,r) = -D\bar{\nabla}N_n(z,r), \tag{14}$$

where D denotes the diffusion coefficient.

Similar equations are set up for the ionic levels. The production is given by electron impact excitation from lower levels, and electron impact de-excitation and radiative decay from higher levels. Cu and Ar impact excitation and de-excitation are not incorporated for the ionic levels. Moreover, ionization from the Cu atomic levels (electron impact ionization, Penning ionization and asymmetric charge transfer) are additional production processes for some ionic levels (i.e., for $n = 9,10,11$; for the explanation, see Sections 2.2.2, 2.2.4 and 2.2.5, respectively), as well as three-body recombination from Cu^{2+} (for the highest excited ionic level, $n = 15$):

$$R_{\text{prod,ions}}(n) = \sum_{l=1}^{n-1} \left[R_{\text{exc,e}}(l)\right] + \sum_{m=n+1}^{N_{\text{tot,ion}}} \left[R_{\text{deexc,e}}(m) + \Lambda(m,n)\cdot A(m,n)\right] + R_{\text{ionize,e}} + R_{\text{PI}} + R_{\text{ACT}} + R_{\text{3b–recom}}. \tag{15}$$

Loss of the ionic levels is caused by electron excitation

to higher ion levels, electron de-excitation and radiative decay to lower ion levels, electron impact ionization to Cu^{2+}, and recombination with electrons to the highest Cu atom level:

$$R_{\text{loss,ions}}(n) = \sum_{m=n+1}^{N_{\text{tot,ion}}} \left[R_{\text{exc,e}}(m)\right] + \sum_{l=1}^{n-1} \left[R_{\text{deexc,e}}(l) + \Lambda(n,l)\cdot A(n,l)\right] + R_{\text{ionize,e}}(\text{to } 16) + + R_{\text{3b–recom}}(\text{to } 8). \quad (16)$$

Transport is given by diffusion and migration in the electric field:

$$\bar{J}_n(z,r) = -D\bar{\nabla}N_n(z,r) - \mu N_n(z,r)\bar{\nabla}V(z,r) \quad (17)$$

where D is again the diffusion coefficient, μ denotes the mobility, and V is the electrical potential.

Finally, for the Cu^{2+} ions, production is caused by electron impact ionization from the Cu atom ground state and from the various Cu^{+} ion levels. The only loss process in the model is three-body recombination to the highest Cu^{+} ion level, and transport is again given by diffusion and by migration in the electric field:

$$R_{\text{prod,Cu}^{2+}} = R_{\text{ionize,e,2}}(\text{from } 1) + \sum_{i=1}^{N_{\text{tot,ion}}} R_{\text{ionize,e}}(i), \quad (18)$$

$$R_{\text{loss,Cu}^{2+}} = R_{\text{3b–recom}}, \quad (19)$$

$$\bar{J}_{\text{Cu}^{2+}}(z,r) = -D\bar{\nabla}N_{\text{Cu}^{2+}}(z,r) - \mu N_{\text{Cu}}2^{+}(z,r)\bar{\nabla}V(z,r). \quad (20)$$

Since the populations of the various levels are determined by the populations of the other levels due to excitation, de-excitation, ionization, recombination and radiative decay, the 16 balance equations for the 16 Cu^{0} atomic and Cu^{+} and Cu^{2+} ionic levels are solved simultaneously at each timestep, until convergence is reached. The differential equations are converted into algebraic equations by the finite difference method, and solved by the Thomas algorithm (which is explained in the appendix of Ref. [23]). A non-uniform spatial grid was used, with most meshpoints adjacent to the cathode. A time-step of 10^{-4} s could be used, and the convergence criterion was fixed at a relative error lower than 10^{-5}.

Data to calculate the Cu atom and ion level populations are the electron energy distribution function and electron density (for electron impact collisions), the energy distributions of plasma species bombarding the cathode (to calculate sputtering), the electric potential (for transport of the Cu ions), the density of Ar ions (for asymmetric charge transfer), of Ar metastable atoms (for Penning ionization) and of Ar ground state atoms (for Ar atom induced collisions), and, of course, basic data (like cross sections and Einstein transition probabilities) for all the processes. The energy distributions and densities of the plasma species, as well as the electric potential, were calculated in our previous models (see Refs. [3–10]) and are used as inputs in the present model. The cross sections and other basic data used in the present model, will be discussed below.

2.2. Discussion of the basic data

2.2.1. Electron impact excitation and de-excitation

Electron impact excitation cross sections for Cu are not so easy to find in the literature compared to, for example, values for Ar. Some data are, however, available in the literature, in connection to copper vapor lasers.

For Cu atoms, a number of papers present cross section data, obtained either experimentally [24–26] or by theoretical calculations [27–30]. However, the data are generally limited to the transitions from the ground level to the $3d^{10}\,4p\,{}^{2}P_{1/2}$ and ${}^{2}P_{3/2}$ levels and to the $3d^{9}\,4s^{2}\,{}^{2}D_{3/2}$ and ${}^{2}D_{5/2}$ levels, which are the upper and lower laser levels, respectively, for the 510.6 and 578.2 nm Cu atom laser lines. Scheibner and Hazi [31] have calculated cross sections for a few more transitions (involving also the $3d^{9}$ 4s 4p quadruplet levels, and the $3d^{10}$ 4d levels) based on 10-state R-matrix close-coupling calculations. Their unpublished data are used in our present collisional–radiative model. The cross sections for other transitions between Cu atom levels, which are not available in the literature, are deduced from the oscillator strengths [32] or from known cross sections between similar transitions in other atoms. For example, the electron impact excitation cross section from $3d^{9}\,4s^{2}\,{}^{2}D_{5/2}$ ($n=2$) to $3d^{9}\,4s^{2}\,{}^{2}D_{3/2}$ ($n=3$) is based on the

form of the cross section for electron excitation from 6^3P_1 to 6^3P_2 in Hg I [33]. Excitation cross sections to and from effective levels are calculated from the individual cross sections as the weighted average over the lower individual levels and the sum over the upper individual levels:

$$\sigma_{\mathrm{exc}}(n,m) = \frac{\sum_x g(x)\left[\sum_y \sigma_{\mathrm{exc}}(x,y)\right]}{\sum_x g(x)}, \qquad (21)$$

where n and m are the lower and upper effective levels, x and y are the corresponding individual levels, and $g(x)$ is the statistical weight of level x.

Fig. 2 shows the electron impact excitation cross sections for all the atomic transitions incorporated in our model, as a function of the electron energy. The cross sections for excitation from the atomic ground state are indicated by solid lines, whereas transitions between excited levels are represented by dashed lines. It is seen that the cross sections are higher for transitions between energy levels lying close to each other (e.g., from 7 to 8, and from 2 to 3). On the other hand, the cross sections for excitation from the ground state to levels 4 and 5 are significantly higher than for excitation to levels 2 and 3, especially at high energies. This phenomenon is made use of in copper vapor lasers, because it gives rise to population inversion of the $3d^{10}$ 4p levels compared to the $3d^9$ $4s^2$ levels, which is the basis for laser action.

For the Cu ions, the excitation cross sections for transitions from the Cu ion ground state ($n = 9$) to the $3d^9$ 4s and $3d^9$ 4p levels ($n = 10$–14) are obtained from a 41-state R-matrix close-coupling calculation [34]. These data were only calculated up to energies of 16 eV; therefore, we fitted some curves of the form A/E^B at about 16 eV and extrapolated them towards higher energies. The cross section for excitation from the Cu ion ground state to the $3d^9$ 5s levels ($n = 15$) is unknown and is therefore assumed to be zero. This approximation is justified, since it concerns an optically forbidden transition for which the cross section, if known, would be low anyhow. Moreover, we have tested that this approximation of using a zero value had no effect on the resulting population density, since other processes (like stepwise excitation from excited Cu^+ levels) are more important.

Since the cross sections for transitions between the Cu ion excited levels are not available in the literature, a simple scaling formula f/E_0^2 (with f and E_0 being the oscillator strength and the threshold energy, respectively) [35] was used to calculate the peak cross section values, with respect to the peak cross section of the resonance transition (from $n = 9$ to $n = 14$), which is known from Ref. [34], i.e.:

$$\sigma_{\mathrm{peak}}(\mathrm{Cu}^{+*}) = \sigma_{\mathrm{peak}}(9 \rightarrow 14)\frac{\left[f/E_0^2\right]_{\mathrm{Cu}^{+*}}}{\left[f/E_0^2\right]_{9\rightarrow 14}}. \qquad (22)$$

The energy dependence of these cross sections is assumed to be the same as for the resonance transition, with the maximum occurring at the threshold energy. It should be mentioned that this method can only be used for optically allowed transitions (for which the oscillator strength is known). The cross sections for optically forbidden transitions are, therefore, assumed to be zero. This is again justified, since these transitions are again negligible compared to other processes. Electronic intermultiplet mixing between Cu ion levels (e.g., $3d^9$ 4s ^{3}D–$3d^9$ 4s ^{1}D) is not taken into account since the cross sections become negligibly small when the electron energies exceed the threshold energy (i.e., 0.1–0.5 eV) by 1–2 orders of magnitude [17].

Fig. 3 presents the electron impact excitation cross sections for all the Cu ion transitions taken into account in our model. Again, the solid lines represent excitation from the Cu ion ground state, whereas the dashed lines indicate the transitions between Cu ion excited levels. The solid lines are characterized by some fine-structure at low energies, which is the result of the detailed 41-state R-matrix close-coupling calculations. At energies above 16 eV, the curves are a simple extrapolation from the lower energies, and no fine-structure is therefore observed. In general, the cross sections used in the model are from fit-equations of the curves in Figs. 2–4. However, this was not possible for excitation from the Cu^+ ion ground state, which shows some fine-structure for energies lower than 16 eV. Therefore, for the latter transitions, the cross sections are directly obtained from look-up tables.

It is seen that the cross section for excitation from the ground state to level $n = 14$ is much higher than to the other levels, which is due to the fact that this

transition is optically allowed. The dashed lines have all the same energy dependence as the resonance transition (9 → 14), as is explained above. The fact that the cross sections for the transitions from 10 and 11 to 13 are higher than the other values is simply due to the fact that level 13 is an effective level consisting of many individual levels (total statistical weight = 52).

The cross sections for electron impact de-excitation, for both the atomic and ionic transitions, are calculated from the corresponding excitation cross sections, based on the principle of detailed balancing:

$$\sigma_{\text{deex,e}}(m,n,E') = \frac{g_n}{g_m}\frac{E}{E'}\sigma_{\text{excit}}(n,m,E), \tag{23}$$

where n and m are the lower and upper level, respectively, g denotes the statistical weight of these levels, and $E' = E - E_{mn}$ (with E_{mn} being the energy difference between level m and level n). To obtain the total de-excitation cross section from an effective level, this cross section is first calculated for each individual level based on the individual excitation cross sections to these levels, with the above formula; then, the total de-excitation cross section from the effective level is computed in the same way as the excitation cross section from an effective level (see above).

2.2.2. Electron impact ionization and electron–ion three-body recombination

The cross section for electron impact ionization from the Cu atom ground state is adopted from the experimental values of Freund [36]. There is not much known about the importance of inner shell ionization (i.e., removal of a $3d^{10}$ electron compared to the 4s electron). We calculated the ratio of both ionization channels with the partial ionization cross sections given by Lotz [37]. It was found that for energies lower than about 60 eV, 4s electron removal is more probable, whereas for higher energies, a 3d electron has more chance to be removed (see also Fig. 4). Indeed, inner shell ionization becomes more important at higher energies, because the more strongly bound electrons can be more easily removed than at low energies. In general, inner shell ionization is less efficient, but the cross section is still considerable, since there are 10 possible d-electrons which can be removed. The partial cross sections were normalized so that the sum of both was equal to the experimental cross section given by Freund [36]. It is clear that the removal of a 4s electron results in the formation of the Cu^+ $3d^{10}$ ground state ($n = 9$), and that the ionization of a $3d^{10}$ electron leads to the Cu^+ $3d^9$ 4s metastable levels ($n = 10$ or 11).

For ionization from the Cu atom excited levels, it is assumed that only the outer (excited) electron can be removed, which is much more weakly bound than the inner shell 3d electrons. The ionization cross sections were deduced from the cross section for removal of the 4s electron from the ground state, with the peak cross sections scaled according to the ratio of the squared threshold energies [38]:

$$\sigma_{\text{peak,Cu}^*} = \sigma_{\text{peak,Cu}^0}\left[\frac{E_{\text{th}}(\text{Cu}^0)}{E_{\text{th}}(\text{Cu}^*)}\right]. \tag{24}$$

The threshold energy for ionization of a Cu excited level ($E_{\text{th}}(\text{Cu}^*)$) is generally smaller than the corresponding value for ionization of the Cu ground state ($E_{\text{th}}(\text{Cu}^0)$); consequently, the ionization cross sections from the Cu excited levels will be higher. This is also visualized in Fig. 4, which presents the ionization cross sections from the Cu atom ground state and excited levels (solid lines). The cross sections for ionization from the $3d^9\,4s^2$ metastable levels ($n = 2$ and 3) and from the $3d^9$ 4s 4p quadruplet levels ($n = 6$) are relatively small compared to the other excited levels, because ionization from these levels leads probably to the formation of the $3d^9$ 4s metastable Cu ion levels ($n = 10$ and 11), since a 4s and a 4p electron will be removed, respectively. Therefore, the threshold energies are slightly higher than for ionization to the Cu ion ground state, and hence the cross section is slightly lower (see Fig. 4). It should also be mentioned that the ionization cross section from the $3d^9\,4s^2$ levels, calculated with the above method, had to be multiplied by two, because there are two 4s electrons which can be removed. Fig. 4 shows also the contribution of ionization of a 4s and a 3d electron from the Cu atom ground state: it follows indeed that a 4s electron can be more easily removed at low energies, whereas the situation is reversed at high energies, as was explained above.

The cross section for electron impact ionization from Cu atoms in the ground state ($n = 1$) to Cu^{2+} ions was adopted from Ref. [36]. As is illustrated in Fig. 4, it is more than an order of magnitude lower than the cross section for ionization to Cu^+ ions.

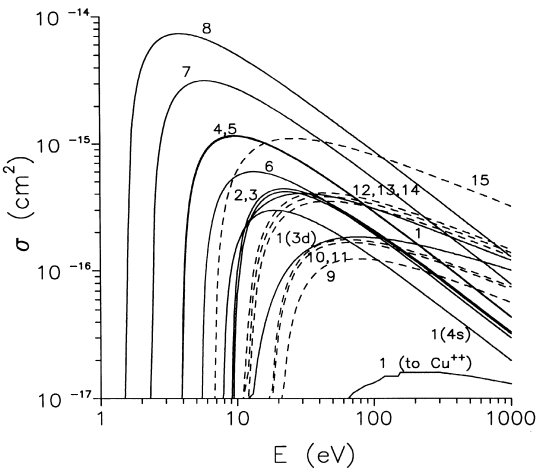

Fig. 4. Cross sections of electron impact ionization for the Cu atom and Cu^+ ion levels, as a function of the electron energy. The cross sections for ionization from the atom levels are indicated with solid lines, while the ionization from the ion levels are presented with dashed lines.

The cross sections for electron impact ionization from Cu^+ ions are represented by the dashed lines in Fig. 4. The cross section for ionization from the ionic ground state was obtained from Ref. [34]. The corresponding values for ionization from the ionic excited levels are again deduced from the cross section for removal of a ground state electron, with the peak cross sections scaled according to the ratio of the squared threshold energies (see above). Again, the higher excited levels have a lower threshold energy, which is manifested in higher cross section values and a maximum at lower energies.

The rate coefficients for three-body recombination between a Cu^+ ion or a Cu^{2+} ion and two electrons are obtained from Ref. [39]:

$$k_{\text{recom}} = 1.154\times10^{-6}\rho T_e^{-5}\ \text{cm}^6\text{s}^{-1} \quad (\textit{for}\ T_e < 3100\ \text{K}),$$
$$k_{\text{recom}} = 7.16\times10^{-4}\rho T_e^{-5.8}\ \text{cm}^6\text{s}^{-1} \quad (\text{for}\ T_e > 3100\ \text{K}), \tag{25}$$

where T_e is the electron temperature and ρ is the Coulomb logarithm:

$$\rho = Z^3 \ln\left[\sqrt{(Z^2+1)}\right], \tag{26}$$

with Z being the charge state of the ion.

This formula is valid for strontium, and in general, it depends on the type of ion. However, since strontium and copper ions have a comparable energy level scheme, the formula can be used for copper as well. At the typical GD-OES discharge conditions under investigation here (i.e., 800 V, 500 Pa, 28 mA), the electron temperature was measured with Langmuir probes to be around 5000 K at ca. 7 mm from the cathode [40]. We are not aware of spatially resolved Langmuir probe measurements in the glow discharge cell under study here (see below); therefore, we use this value throughout the whole discharge. This is only an approximation, but it affects only the highest excited Cu^+ ion level (see Table 2), which has no significant influence on the other levels. Hence, the recombination rate coefficients are calculated to be $8.7\times10^{-26}\ \text{cm}^6\,\text{s}^{-1}$ (for $Cu^+/2e^-$) and $1.6\times10^{-24}\ \text{cm}^6\,\text{s}^{-1}$ (for $Cu^{2+}/2e^-$). As mentioned before, it is assumed that recombination leads to atoms (in the case of $Cu^+/2e^-$) or ions (in the case of $Cu^{2+}/2e^-$) in the highest excited level, i.e., level $n = 8$ and $n = 15$, respectively.

2.2.3. Ar or Cu atom impact excitation and de-excitation

Cross sections for excitation and de-excitation due to collisions with Ar or Cu atoms are, to our knowledge, only available for some reactions concerning the Cu atom $3d^9\,4s^2\,{}^2D$ levels ($n = 2$ and 3) and the $3d^{10}\,4p\,{}^2P$ levels ($n = 4$ and 5) [41]: i.e., for collisional mixing (= excitation and de-excitation) within the ^2D or ^2P levels by collisions with both Ar or Cu atoms, and for collisional quenching (= de-excitation) of these levels towards the ground state due to Ar or Cu atoms.

Collisional quenching from the ^2P levels to the ground state can, however, completely be neglected compared to radiative decay from these levels. Moreover, collisional mixing within these levels is also neglected, because the energy difference is only 0.03 eV, and such collisions will not perturb the level populations (i.e., the ratio of their densities is only determined by their statistical weights, i.e., 1:2). Hence, this leaves us with collisional mixing and quenching of the ^2D levels due to both Cu or Ar atoms. The following reaction channels are incorporated in the model, with the cross sections adopted

Table 2
Calculated relative contributions of the various populating and depopulating processes for the Cu atomic and ionic levels, integrated over the entire three-dimensional discharge region

Level number	Populating processes (%)	Depopulating processes (%)
1 Cu^0 $3d^{10}\ 4s\ ^2S_{1/2}$	Sputtering (98.7) Radiative decay from $n = 4$ (0.4) Radiative decay from $n = 5$ (0.6) Electron impact de-excitation from $n = 2$ (0.2) Electron impact de-excitation from $n = 3$ (0.1)	Penning ionization (66.4) Asymmetric charge transfer (16.1) Electron impact ionization (4s electron) (2.1) Electron impact ionization (3d electron) (1.1) Electron impact excitation to $n = 2$ (0.9) Electron impact excitation to $n = 3$ (0.6) Electron impact excitation to $n = 4$ (3.8) Electron impact excitation to $n = 5$ (7.5) Electron impact excitation to $n = 6$ (0.4) Electron impact excitation to $n = 8$ (1.1)
2 Cu^0 $3d^9\ 4s^2\ ^2D_{5/2}$	Electron impact de-excitation from $n = 3$ (69) Electron impact de-excitation from $n = 5$ (0.2) Cu^0 impact de-excitation from $n = 3$ (2.5) Electron impact excitation from $n = 1$ (4.6) Radiative decay from $n = 5$ (22.4) Radiative decay from $n = 6$ (0.9) Radiative decay from $n = 8$ (0.4)	Electron impact excitation to $n = 3$ (93.7) Electron impact excitation to $n = 6$ (0.4) Electron impact de-excitation to $n = 1$ (5.0) Cu^0 impact excitation to $n = 3$ (0.1) Electron impact ionization (0.4)
3 Cu^0 $3d^9\ 4s^2\ ^2D_{3/2}$	Electron impact excitation from $n = 2$ (80.3) Electron impact excitation from $n = 1$ (3.4) Electron impact de-excitation from $n = 4,5$ (0.2) Cu^0 impact excitation from $n = 2$ (0.1) Radiative decay from $n = 4$ (11.7) Radiative decay from $n = 5$ (3.4) Radiative decay from $n = 6$ (0.6) Radiative decay from $n = 8$ (0.3)	Electron impact de-excitation to $n = 2$ (92.1) Electron impact de-excitation to $n = 1$ (4.2) Cu^0 impact de-excitation to $n = 2$ (3.3) Electron impact ionization (0.1)
4 Cu^0 $3d^{10}\ 4p\ ^2P_{1/2}$	Electron impact excitation from $n = 1$ (92.0) Radiative decay from $n = 7$ (0.6) Radiative decay from $n = 8$ (7.3)	Radiative decay to $n = 1$ (49.5) Radiative decay to $n = 3$ (48.7) Electron impact de-excitation to $n = 1$ (1.2)
5 Cu^0 $3d^{10}\ 4p\ ^2P_{3/2}$	Electron impact excitation from $n = 1$ (92.0) Electron impact excitation from $n = 2$ (0.1) Radiative decay from $n = 7$ (0.6) Radiative decay from $n = 8$ (7.3)	Radiative decay to $n = 1$ (35.5) Radiative decay to $n = 2$ (55.4) Radiative decay to $n = 3$ (7.1) Electron impact de-excitation to $n = 1$ (1.4) Electron impact de-excitation to $n = 2$ (0.4)
6 Cu^0 $3d^{10}\ 4s\ 4p$ $^4P, ^4D, ^4F$	Electron impact excitation from $n = 1$ (79.4) Electron impact excitation from $n = 2$ (13.5) Electron impact excitation from $n = 3$ (7.1)	Radiative decay to $n = 1$ (30.2) Radiative decay to $n = 2$ (39.6) Radiative decay to $n = 3$ (24.0) Electron impact de-excitation to $n = 1$ (0.2) Electron impact de-excitation to $n = 2$ (2.7) Electron impact de-excitation to $n = 3$ (3.0) Electron impact de-excitation to $n = 4,5$ (0.2)
7 Cu^0 $3d^{10}\ 5s\ ^2S_{1/2}$	Radiative decay from $n = 8$ (83) Electron impact excitation from $n = 4$ (3.4) Electron impact excitation from $n = 5$ (7.4) Electron impact de-excitation from $n = 8$ (6.2)	Radiative decay to $n = 4$ (32.6) Radiative decay to $n = 5$ (66.6) Electron impact de-excitation to $n = 4$ (0.3) Electron impact de-excitation to $n = 5$ (0.5)

8	Electron impact excitation from $n = 1$ (98.1)	Radiative decay to $n = 1$ (1.8)
Cu^0	Electron impact excitation from $n = 2$ (0.4)	Radiative decay to $n = 2$ (8.0)
$3d^{10}$ 5p, 3d	Electron impact excitation from $n = 3$ (0.1)	Radiative decay to $n = 3$ (3.8)
	Electron impact excitation from $n = 4$ (0.1)	Radiative decay to $n = 4$ (27.1)
	Electron impact excitation from $n = 5$ (0.2)	Radiative decay to $n = 5$ (53.8)
	Electron–ion three-body recombination (1.1)	Radiative decay to $n = 7$ (5.1)
		Electron impact de-excitation to $n = 7$ (0.4)
9	Penning ionization (89.1)	Electron–ion three-body recombination (14.5)
Cu^+	Electron impact ionization (4.8)	Electron impact ionization (10.8)
$3d^9$ 4s $^1S_0$	Electron impact de-excitation from $n = 10$ (5.5)	Electron impact excitation to $n = 10$ (18.1)
	Electron impact de-excitation from $n = 11$ (0.5)	Electron impact excitation to $n = 11$ (12.5)
		Electron impact excitation to $n = 12$ (1.5)
		Electron impact excitation to $n = 13$ (6.6)
		Electron impact excitation to $n = 14$ (36)
10	Penning ionization (54.1)	Electron impact de-excitation to $n = 9$ (95.9)
Cu^+	Electron impact ionization (2.4)	Electron impact excitation to $n = 12,13,14$ (3.6)
$3d^9$ 4s $^3D_{3,2,1}$	Radiative decay from $n = 12$ (43.2)	Electron–ion three-body recombination (0.2)
	Radiative decay from $n = 13$ (0.2)	Electron impact ionization (0.2)
11	Penning ionization (94.2)	Electron impact de-excitation to $n = 9$ (96)
Cu^+	Electron impact ionization (4.2)	Electron impact excitation to $n = 12,13,14$ (3.6)
$3d^9$ 4s $^1D_2$	Radiative decay from $n = 12$ (1.1)	Electron–ion three-body recombination (0.2)
	Radiative decay from $n = 13$ (0.3)	Electron impact ionization (0.2)
12	Asymmetric charge transfer (99.99)	Radiative decay to $n = 10$ (99.4)
Cu^+3d^9 4p $^3P_2$		Radiative decay to $n = 11$ (0.5)
13	Electron impact excitation from $n = 9$ (2.5)	Radiative decay to $n = 10$ (78.3)
Cu^+	Electron impact excitation from $n = 10$ (89.5)	Radiative decay to $n = 11$ (21.5)
$3d^9$ 4p (other)	Electron impact excitation from $n = 11$ (7.8)	
	Radiative decay from $n = 15$ (0.2)	
14	Electron impact excitation from $n = 9$ (95.5)	Radiative decay to $n = 9$ (76.8)
Cu^+	Electron impact excitation from $n = 10$ (0.7)	Radiative decay to $n = 10$ (1.5)
$3d^9$ 4p $^1P_1$	Electron impact excitation from $n = 11$ (3.7)	Radiative decay to $n = 11$ (21.6)
15	Electron–ion three-body recombination (95.8)	Radiative decay to $n = 12$ (12.2)
Cu^+	Electron impact excitation from $n = 12$ (4.2)	Radiative decay to $n = 13$ (82.5)
$3d^9$ 5s		Radiative decay to $n = 14$ (5.0)
16	Electron impact ionization from $n = 1$ (87.0)	Electron–ion three-body recombination (100)
Cu^{2+}	Electron impact ionization from $n = 9$ (4.9)	
	Electron impact ionization from $n = 10$ (7.4)	
	Electron impact ionization from $n = 11$ (0.7)	

from [41]:

$$Cu^*(3d^9\ 4s^2\ ^2D_{5/2})(n = 2) + Ar^0 \rightarrow Cu^0(3d^{10}\ 4s\ ^2S_{1/2})(n = 1) + Ar^0 + \Delta E,$$

$\sigma_{quench,Ar(2-1)} \leq 10^{-21}\ cm^2$;

$$Cu^*(3d^9\ 4s^2\ ^2D_{3/2})(n = 3) + Ar^0 \rightarrow Cu^0(3d^{10}\ 4s\ ^2S_{1/2})(n = 1) + Ar^0 + \Delta E,$$

$\sigma_{quench,Ar(3-1)} \leq 10^{-21}$ cm^2;

$Cu^*(3d^9\ 4s^2\ ^2D_{5/2})(n=2) + Cu^0$

$\rightarrow Cu^0(3d^{10}\ 4s\ ^2S_{1/2})(n=1) + Cu^0 + \Delta E$,

$\sigma_{quench,Cu(2-1)} = 4.8 \times 10^{-17}$ cm^2;

$Cu^*(3d^9\ 4s^2\ ^2D_{3/2})(n=3) + Cu^0$

$\rightarrow Cu^0(3d^{10}\ 4s\ ^2S_{1/2})(n=1) + Cu^0 + \Delta E$,

$\sigma_{quench,Cu(3-1)} = 4.8 \times 10^{-17}$ cm^2;

$Cu^*(3d^9\ 4s^2\ ^2D_{3/2})(n=3) + Ar^0$

$\Leftrightarrow Cu^0(3d^9\ 4s^2\ ^2D_{5/2})(n=2) + Ar^0 + \Delta E$,

$\sigma_{mix,Ar(3-2)} \leq 10^{-20}$ cm^2;

$Cu^*(3d^9\ 4s^2\ ^2D_{3/2})(n=3) + Cu^0$

$\Leftrightarrow Cu^0(3d^9\ 4s^2\ ^2D_{5/2})(n=2) + Cu^0 + \Delta E$,

$\sigma_{mix,Cu(3-2)} = 1.7 \times 10^{-15}$ cm^2.

The cross sections for the reverse collisional mixing processes (i.e., excitation from level 2 to level 3) by Ar and Cu atoms are obtained from the formula for detailed balancing (see Section 2.2.1). The energy difference between $n = 2$ and $n = 3$ is 0.253 eV. Since both the Cu and Ar atoms are assumed to be characterized by thermal energy, with a mean value of 0.1 eV (which corresponds to the assumed gas temperature of 800 K; see above), only a fraction of these atoms, with an energy higher than this threshold is able to cause excitation. This fraction is calculated from the Maxwell–Boltzmann distribution to be about 7%.

It can be seen that the above cross sections for collisions with the Ar atoms are much lower (the values used in the model are the upper limits) than the corresponding values for Cu atoms. However, the Ar atoms have a higher density than the Cu atoms (i.e., ca. 10^{16}–10^{17} cm^{-3} compared to ca. 10^{14} cm^{-3} at the typical discharge conditions under study [21]), so that both reaction channels are incorporated.

2.2.4. Penning ionization

The rate coefficient for Penning ionization between Cu atoms and Ar metastable atoms is not directly available from the literature. However, in Ref. [42] an empirical formula is given relating the Penning ionization cross section to the reduced mass and the atomic radii of the collision partners. We fitted this empirical formula to some experimental cross section data available in the literature (e.g., Refs. [42, 43]), in order to arrive at approximate values for other elements. In this way, the Penning ionization cross section of Cu atoms with Ar metastable atoms was computed to be 4.9×10^{-15} cm^2 at thermal energies, which corresponds to a rate coefficient of 2.36×10^{-10} cm^3 s^{-1}.

Further, it is not exactly known whether the Cu ion is formed in the ground state or in excited levels by this Penning ionization process. In Ref. [44] it was stated that, on one hand, the rate of this process is proportional to

$$W(R) = 1/\hbar \left| \langle A^{+*}, B, e | V(R) | A, B^* \rangle \right|^2 \rho_f(E),$$

where R is the internuclear distance, $V(R)$ is the interaction potential, $\langle A^{+*},B,e|$ and $|A,B^*\rangle$ are the relevant wave functions, and $\rho_f(E)$ is the final density of states, which is essentially that of the ejected electrons. It is proportional to the matrix element of the transition which has a resonant character, i.e., it is large mainly at low energies of the ejected electrons. On the other hand, the rate is also proportional to $\rho_f(E)$, which increases with the electron energy. It is the competition between these two above-mentioned factors which determines the magnitude of this process.

Inaba et al. have investigated the relative rates for Penning ionization to individual excited ion levels, by means of Penning electron spectroscopy for Cd, Zn and Mg atoms with He or Ne metastable atoms [43, 45–48]. They found that about 60% of the ions are formed in the ground state, whereas the remaining fraction is distributed over the excited levels with energies lower than the He or Ne metastable level energy. A similar study was performed by Baltayan et al. [49, 50] in a flowing afterglow apparatus, for He metastable atoms with Cd or Zn atoms; it was found that for He–Cd ca. 40% leads to ions in the ground state, while for He–Zn about 90% of the ions are formed in the ground level.

Based on all these observations, we assumed that for Penning ionization between Ar metastable atoms and Cu atoms, 60% of the Cu ions are formed in the ground state. The remaining 40% leads to Cu ions in

excited levels lying below the Ar metastable levels (i.e., at 11.55 and 11.72 eV). This is only the case for the four $3d^9$ 4s levels. Therefore we assume that 10% goes to each of these levels. Since the $3d^9$ 4s $^3D_1$, $^3D_2$ and $^3D_3$ levels are combined into an effective level ($n = 10$), this corresponds to a distribution of 30% to level $n = 10$ and 10% to level $n = 11$.

2.2.5. Asymmetric charge transfer

The rate coefficient for asymmetric charge transfer between Ar ions and Cu atoms is even more difficult to find in the literature. Data for this process at thermal energies between rare gases and metal atoms are only available for specific combinations of reactants, like He^+–Cd [50–52], He^+–Zn [49], He^+–Hg [53–59], He^+–Cs [60], He^+–Rb [61], Ne^+–Zn [62], etc., in connection with metal–vapor ion lasers. It is generally known that this process is only significant when the energy difference between the levels of the rare gas and metal ion is sufficiently small (i.e., good energy overlap). However, the process is quite complicated; for example, it is not always true that the smallest energy difference between energy levels yields the highest cross section [49, 53, 63]. Therefore, it is almost impossible to deduce the cross section for a specific combination of reactants from data between other elements.

In Refs. [49, 50] cross section data are available for both Penning ionization and asymmetric charge transfer of He metastable atoms or He ions, respectively, with Cd and Zn atoms. In these cases, a good energy overlap was found for asymmetric charge transfer, and moreover, the cross sections for Penning ionization and asymmetric charge transfer were measured to be of comparable magnitude. For the Ar^+–Cu system under study here, there are no Cu ion levels showing good overlap with the Ar ion ground state ($3p^5\ ^2P_{3/2}$, at 15.76 eV), but there is one Cu ion level which lies only slightly above the Ar ion metastable level ($3p^5\ ^2P_{1/2}$, at 15.94 eV), i.e. the $3d^9$ 4p $^3P_2$ level ($n = 12$), at 15.96 eV. These two Ar ion levels are, actually, two different ionization limits for Ar, corresponding to the primed and unprimed system, and it is assumed that their densities are in the same ratio as their statistic weights, i.e. $Ar^+/Ar_m^+ \sim 4/2$. In our model network, we have calculated only the total Ar ion density [5, 9]. Hence, the densities of the Ar ion ground and metastable levels are considered to be 2/3 and 1/3 of our total calculated Ar ion density, respectively (in the assumption that the other excited Ar ion levels have much lower densities and can be neglected) [12, 14, 19]. Since there is good energy overlap between the Ar ion metastable level and the $n = 12$ Cu ion level, we assume that the rate coefficient of asymmetric charge transfer is the same as the one for Penning ionization, i.e., $k_{ACT} = 2.36 \times 10^{-10}\ cm^3\ s^{-1}$. This value is in reasonable agreement with the value of $2 \times 10^{-10}\ cm^3\ s^{-1}$, obtained by fitting modeling results of an Ar–Cu ion vapor laser to experimental data in Ref. [64].

We assume that all ions are formed in the $n = 12$ Cu ion level by this process, and not into other levels. Indeed, Steers has demonstrated that in an argon discharge, the intensity of the 224.7 nm line, originating from the $3d^9$ 4p $^3P_2$ level, is significantly higher than other lines originating from nearby levels, compared to a neon or helium discharge; this was attributed to the selective ionization/excitation of the $^3P_2$ level by asymmetric charge transfer with Ar, at typical GD-OES discharge conditions [19].

Another reaction channel of asymmetric charge transfer for Ar^+–Cu, which would be possible based on energy considerations, is between the Ar ion ground state and the Cu atom metastable levels ($n = 2$ and 3) [64]. However, this would yield selective excitation of other Cu ion levels, and it was found in Ref. [19] that lines originating from these other levels are not particularly intense at typical GD-OES conditions. Therefore, the latter reaction channel is neglected in our model.

2.2.6. Radiative decay

The Einstein transition probabilities, which determine the rate of radiative decay, are adopted from Refs. [28, 65] for the Cu atoms and from [17, 66] for the Cu^+ ion transitions. The transition probabilities from and towards effective levels were calculated from the individual values by [14]:

$$\bar{A}(m,n) = \frac{\sum_x \sum_y g(y)A(y,x)}{\sum_y g(y)}, \qquad (27)$$

where n and m are the lower and upper effective levels, and x and y are the individual levels belonging to the lower and upper effective levels, respectively.

The net rate of radiative decay is, however, not only determined by the Einstein transition probability, but the latter must be multiplied by a so-called escape factor. Indeed, a fraction of the emitted radiation from an upper to a lower level can again be absorbed by the lower level, leading to re-excitation from the lower to the upper level, i.e., called 'radiation trapping' or 'photo-excitation'. In this way, the complex problem of describing radiation transfer is avoided.

The escape factor expresses the fraction of photons which are not re-absorbed by the lower level, but which can escape from the discharge plasma. It is calculated as follows [12, 14, 67–69]. For a cylindrical tube of radius R, and when both Doppler and collisional line broadening are present, it holds:

$$\Lambda(m,1) = 1.9T_D \exp\left(\frac{-\pi T_{CD}^2}{4T_C^2}\right) + 1.3T_C \operatorname{erf}\left(\frac{\sqrt{\pi}T_{CD}}{2T_C}\right), \quad (28)$$

where T_D and T_C are the transmission coefficients for pure Doppler and collisional broadening, respectively, and T_{CD} is the coefficient for collisionally broadened emission and Doppler broadened absorption profiles:

$$T_D = \frac{1}{k_0 R\sqrt{\pi \ln(k_0 R)}}, \quad (29)$$

$$T_C = \sqrt{\frac{a}{\sqrt{\pi}k_0 R}}, \quad (30)$$

$$T_{CD} = \frac{2a}{\pi\sqrt{\ln(k_0 R)}}, \quad (31)$$

where k_0R is the optical depth pertaining to the line center and a is the damping coefficient:

$$k_0 R = \frac{3.323\times10^{-18}}{[E_{excit}(m)]^3}\frac{g(m)}{g(n)}\sqrt{\frac{M_a}{T_a}}A(m,n)N_n R, \quad (32)$$

$$a = A(m,n)\left[1 + \frac{3.225\times10^{-14}}{[E_{excit}(m)]^3}\frac{g(m)}{g(n)}N_n\right] \times \frac{7.657\times10^{-10}}{E_{excit}(m)}\sqrt{\frac{M_a}{T_a}}, \quad (33)$$

where $E_{excit}(m)$ and $g(m)$ are the excitation energy and statistical weight of upper level m, respectively, $g(n)$ is the statistical weight of lower level n, $A(m,n)$ is the Einstein transition probability for radiative decay from level m to level n, T_a and M_a are the atom temperature and mass, respectively, R is the radius of the cell cylinder (i.e., different value for the narrow neck near the cathode ($R = 0.4$ cm) and for the main volume ($R = 1.6$ cm); see Fig. 5 below), and N_n is the number density of the lower level. The latter quantity varies as a function of axial and radial position. However, the above formulas take the integral over all directions in which the photons can escape. Therefore, the density of the lower level at each position is averaged over all nearby positions.It is clear that the above formulas can only be used when $k_0R > 1$. Indeed, in a very simplified case, the re-absorption is weakened as e^{-k_0R}, where k_0^{-1} symbolizes the 'mean free path of a photon', If $k_0R < 1$, it holds that the cell radius $R < k_0^{-1}$ and that no re-absorption will take place. The condition of $k_0R > 1$ is satisfied when N_n is sufficiently large. Indeed, if the lower level density is rather low, there will be no re-absorption. It was found that at the discharge conditions under study, only the Cu atom ground state density close enough to the cathode was sufficiently high to re-absorb a fraction of the emitted photons, so that the above formulas are only used for the lower level equal to the Cu atom ground state. For transitions to all other levels (Cu atom excited levels, and Cu ion levels), the escape factor is simply assumed to be equal to 1 (i.e., 100% escape of radiation, no radiation trapping).

2.2.7. Transport by diffusion and migration

The diffusion coefficient of the Cu atoms in argon is calculated with a formula of the rigid-sphere model for a mixture of two chemical species [70], which yields $D = 144.6\ \mathrm{cm^2\,s^{-1}}$ at 1 Torr argon and 300 K. In a first approximation it can be assumed that diffusion is not determined by the charge of a particle; therefore, the diffusion coefficient of the Cu^+ and Cu^{2+} ions is taken equal to that of the Cu atoms. Moreover, the same value is also used for the Cu atoms and ions in excited levels.

The mobility of the Cu^+ ions is adopted from Ref. [71] where a graph of the mobility as a function of the ion mass in argon, neon and helium was presented. It was taken to be $1837.4\ \mathrm{cm^2\,s^{-1}}$ at 1 Torr argon and

300 K. Again, the same value is used for the Cu^+ ions in the ground state and also in the excited levels. The mobility of the Cu^{2+} ions is assumed to be two times the value of the Cu^+ ions, based on the effect of the double charge.

2.2.8. Sputtering

The sputtering term in Eq. (12) consists of J_0 (= the flux of sputtered Cu atoms from the cathode) multiplied by F_T (= the three-dimensional thermalization profile of the sputtered Cu atoms). Indeed, when the sputtered Cu atoms leave the cathode, they have energies of 5–15 eV [72]. They lose these energies almost immediately by collisions with the Ar gas atoms until they are thermalized, after which they diffuse further into the plasma or back towards the cathode. Since thermalization is much faster than diffusion, it can be assumed already finished when diffusion starts [73]. Therefore, both processes can be separated in time when modeling the behavior of the sputtered atoms, i.e., the simulation of the thermalization process results in a thermalization profile, which is used afterwards as starting distribution for the further diffusion process. The description of the thermalization is carried out with a Monte Carlo model, as is explained in detail in Ref. [4].

J_0 is determined from an empirical formula for the sputtering yield [74], multiplied by the flux energy distributions of the plasma species bombarding the cathode (i.e., Ar ions, fast Ar atoms and also Cu ions). The latter are calculated with Monte Carlo models in the cathode dark space [3, 7–10]. This sputtering term is only used for the Cu atoms in the ground state. Indeed, it may be possible that the Cu atoms are sputtered in the form of excited levels, but they will probably be de-excited by collisions with the Ar gas atoms so that the thermalization profile exists only of ground state Cu atoms.

2.2.9. Boundary conditions

Finally, the boundary conditions for this set of equations are determined by the sticking coefficients of the Cu atoms and ions at the walls. For the Cu atoms in the ground state, a sticking coefficient of 0.5 was used (i.e., 50% of the atoms are adsorbed at the walls) [10], whereas for the excited Cu atoms and the Cu ions, the sticking coefficient was assumed to be 1 (i.e., 100% will be de-excited and/or neutralized when they collide with the surface, and 'disappear as such' from the plasma).

3. Results and discussion

The calculations are carried out at typical conditions used for GD-OES, i.e., 800 V, 500 Pa, 28 mA, and in a discharge cell which is used in all commercial GD-OES instruments, i.e., the so-called Grimm cell. This cell has a length of 7.8 cm and an overall diameter of 1.6 cm. However, close to the cathode, the diameter is only 0.4 cm. A schematic picture of this cell is presented in Fig. 5 [21]. Due to the cylindrical symmetry of this cell, the calculations could be performed in two dimensions (radial and axial direction).

3.1. Level population densities

3.1.1. Cu atom two-dimensional density profile

Fig. 6 presents the two-dimensional population density of the Cu atom ground state ($n = 1$). The cathode of the cell is given by the left border of the plot, whereas the anode cell body is represented by the other borders, as well as the gray rectangles. The density reaches a maximum adjacent to the cathode (due to sputtering at the cathode) and decreases further into the cell. An expanded view is included in the figure to present a detail of the profile in the narrow neck close to the cathode. The Cu atom excited levels ($n = 2$–8) are characterized by exactly the same profile, but the absolute values are some orders of magnitude lower. Since the absolute values at the maximum of the profiles are presented below (see Fig. 8), the two-dimensional profiles give no additional information and are, therefore, not shown here. The density profile of sputtered metal ground state atoms in a glow discharge has been measured by laser induced fluorescence and by atomic absorption spectrometry, for a somewhat different cell geometry, slightly different discharge conditions and another element (tantalum, because of availability of laser wavelengths) [75]. The results were in very good agreement with our calculation results for exactly the same conditions and cell geometry and also tantalum as cathode material. These results were based on a slightly different model from the present one (i.e., an earlier version, considering only the sputtered

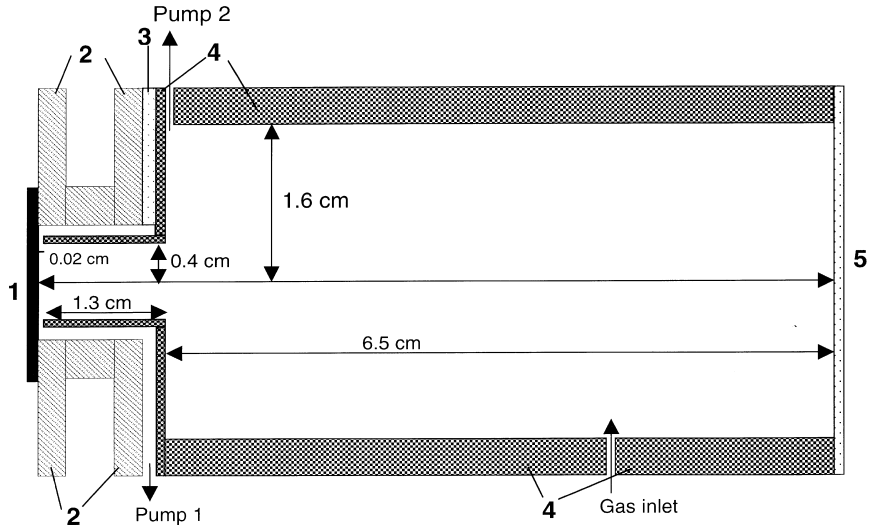

Fig. 5. Schematic representation of the Grimm source geometry, used in the model. (1) Sample, (2) cathode, (3) insulator, (4) anode cell body, (5) quartz window. Reprinted from Ref. [21] with permission of Elsevier Science.

atoms and ions in the ground state, and no excited levels), but the results of both models concerning the sputtered ground state atom densities (when both models deal with copper) are exactly the same. This suggests that the present model will also yield realistic results. Moreover, Hoffmann et al. measured lateral distributions (end-on observation) of emission line intensities of sputtered atoms in the same cell geometry as used for the model, and they obtained a parabolic profile with the maximum at the cell axis if the atoms were distributed homogeneously over the sample surface [76]. This characteristic parabolic profile is also found back in our calculations of the sputtered atom excited levels (which give rise to the emission line profiles).

3.1.2. Cu^+ ion two-dimensional density profile

The two-dimensional population density of the Cu^+ ion ground state ($n = 9$) is illustrated in Fig. 7. The density reaches a maximum at about 2 mm from the cathode (i.e., in the beginning of the negative glow region, see Ref. [21]) and decreases also further in the cell. A detail of the profile close to the cathode, is again presented in the expanded view. This population profile is also characteristic for the profiles of the excited Cu^+ ion levels and the Cu^{2+} ions; only the absolute values are lower, as will be shown in Fig. 8. The two-dimensional profiles of the other levels are, therefore, not presented here. Again, we have measured two-dimensional density profiles of sputtered tantalum ground state ions by laser induced fluorescence [75] and the results were also in good agreement with the calculation results for tantalum ions, which suggests that the present results will also be reliable.

3.1.3. Cu atom, Cu^+ and Cu^{2+} ion densities at the maximum

The values at the maximum of the profiles, for all Cu atom and Cu^+ ion levels and for the Cu^{2+} ions, are depicted in Fig. 8 (solid line, left axis). As was shown already in Fig. 6, the Cu atom ground state ($n = 1$) has a population of about 2×10^{14} cm^{-3} at its maximum. This is about two orders of magnitude higher than the population of the two lowest excited levels (i.e., the $3d^9\,4s^2$ levels; $n = 2$ and 3), which have a maximum density in the order of 10^{12} cm^{-3}. The latter is still clearly higher than the other excited levels. Indeed, the two $3d^9\,4s^2$ levels are metastable levels, i.e., they cannot decay to the ground state by emission of radiation, which explains their relatively high density. The $3d^{10}$ 4p levels ($n = 4$ and 5) have a maximum population density of 3 and 6×10^{10} cm^{-3} (for the $^2P_{1/2}$ and $^2P_{3/2}$ levels, respectively). This relative ratio of both

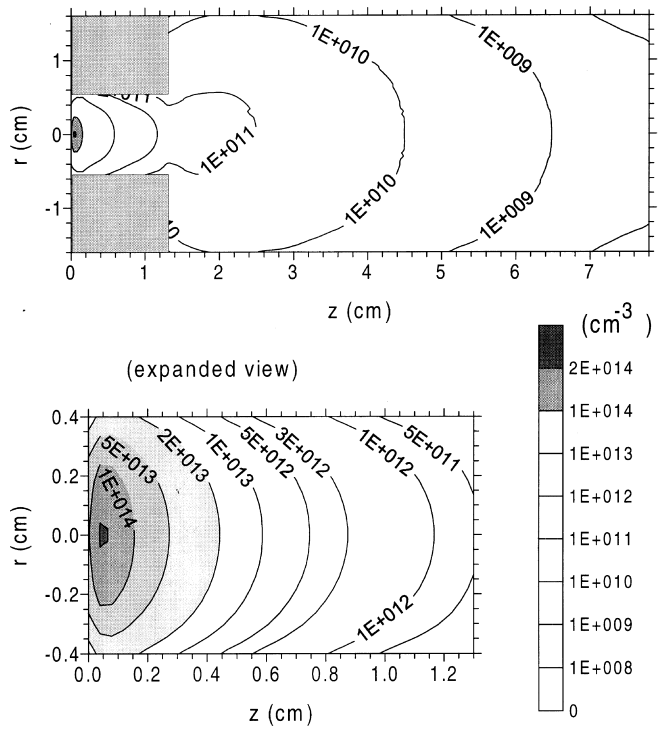

Fig. 6. Two-dimensional density profile of the Cu atom ground state throughout the discharge. The cathode of the cell is at $z = 0$ cm, the anode cell body is represented by the other borders of the figure, as well as by the gray rectangles from $z = 0$ to 1.3 cm. Included is also an expanded view of the region close to the cathode

levels is in excellent agreement with their statistical weights. From Fig. 8 follows that the higher excited levels have still lower population densities, as is explained by the increasing excitation energy of these levels (see dashed line, right axis). Level $n = 6$ (i.e., the $3d^9$ 4s 4p quadruplet levels) is an effective level in the model. The populations of the individual levels belonging to this effective level were calculated from the ratio of their statistical weights to the total statistical weight; they vary between 4×10^8 cm^{-3} (e.g., for $^4P_{1/2}$ and $^4D_{1/2}$; $g = 2$) and 2×10^9 cm^{-3} (for $^4F_{9/2}$; $g = 10$). This 'population range' is indicated in Fig. 8. The $3d^{10}$ 5s level ($n = 7$) has a population density of ca. 3×10^8 cm^{-3} at the maximum of its profile. This is slightly lower than for the quadruplet ($n = 6$) levels, which is attributed to the slightly higher excitation energy and (compared to some but not all of the quadruplet levels) to the lower statistical weight. The $n = 8$ level is again an effective level. The individual level populations were again calculated based on their statistical weights; they are ca. 3.5×10^7 cm^{-3} for 5p $^2P_{1/2}$ ($g = 2$), ca. 7×10^7 cm^{-3} for 5p $^2P_{3/2}$ and for 4d $^2D_{3/2}$ and ca. 10^8 cm^{-3} for 4d $^2D_{5/2}$ ($g = 6$), as is presented in Fig. 8. In general, the decreasing trend as a function of level number and the logarithmic scale demonstrate that by far most of the Cu atoms are found in the ground state at these glow discharge conditions.

The Cu^+ ion ground state ($n = 9$) has a maximum density of about 2×10^{12} cm^{-3}, as appeared also from Fig. 7. This is about two orders of magnitude lower than the Cu atom density, which indicates that the ionization degree of the sputtered Cu atoms is in the percent order at the present discharge conditions. The $3d^9$ 4s levels ($n = 10$ and 11) have only a slightly lower population density, i.e., ranging from 3×10^{11} to 8×10^{11} cm^{-3} for the $^3D_{1,2,3}$ levels (according to their statistical weight) and about 1.5×10^{11} cm^{-3} for the $^1D_2$ level. Indeed, it is assumed in our model that the $3d^9$ 4s levels can also directly be formed by ionization of the Cu atoms (by electron impact and Penning ionization; see above), and they are not

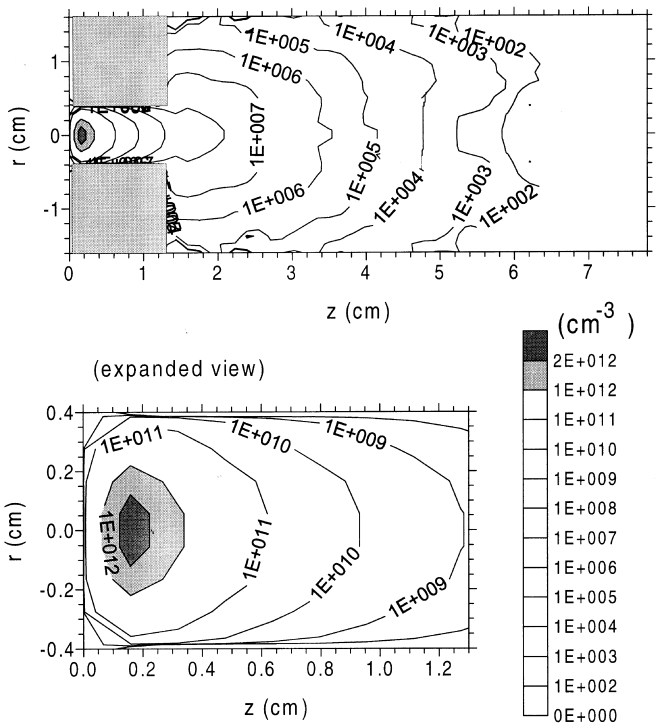

Fig. 7. Two-dimensional density profile of the Cu^+ ion ground state throughout the discharge. The cathode of the cell is at z = 0 cm, the anode cell body is represented by the other borders of the figure, as well as by the gray rectangles from $z = 0$ to 1.3 cm. Included is also an expanded view of the region close to the cathode

able to decay to the Cu^+ ion ground state by emission of radiation (metastable levels). The other excited Cu^+ ion levels are not metastable, and this is reflected in their much lower population density. The density of the $3d^9\ 4p\ ^3P_2$ level ($n = 12$) is, however, still rather high, because it follows from the model that it is very efficiently created by asymmetric charge transfer of Cu atoms with Ar ions (see above, and also Table 2). This high density can indeed explain the anomalously high intensity of the 224.7 nm line originating from this level, as was observed for typical GD-OES discharge conditions by Steers et al. [19]. The other $3d^9$ 4p levels have clearly lower population densities, ranging from $10^5\ cm^{-3}$ to $9 \times 10^5\ cm^{-3}$ for the $n = 13$ levels (depending on the statistical weights), and about $6 \times 10^5\ cm^{-3}$ for the $3d^9\ 4p\ ^1P_1$ level ($n = 14$). The latter population density is a factor of three higher than the corresponding values for the $n = 13$ levels with the same statistical weight (e.g., the $^3P_1$ level), which is attributed to the efficient electron impact excitation from the Cu^+ ion ground state. The population densities of the $3d^9$ 5s levels are again about two orders of magnitude lower (i.e. 2–$5 \times 10^3\ cm^{-3}$), due to the clearly higher excitation energies.

Finally, the Cu^{2+} ion density ($n = 16$) was calculated to be $3.4 \times 10^9\ cm^{-3}$ at the maximum of its profile, as appears from Fig. 8. It should be mentioned that this value represents the total Cu^{2+} ion density (i.e., the sum of all levels). The ratio of Cu^{2+} to Cu^+ density is hence about 10^{-2}, which is the same as for the ratio of Cu^+ ion to Cu atom density.

In order to investigate whether the excited Cu atom and Cu^+ ion levels are populated according to the Boltzmann distribution, we have also plotted the density per statistical weight of the various levels as a function of excitation energy. The result is shown in Fig. 9. For the Cu atoms, a more or less straight line can be observed, although the $3d^{10}$ 4p levels ($E = 3.8$ eV) seem to be somewhat overpopulated and the $3d^{10}$ 5s level is clearly underpopulated. The reason for this is clear: the $3d^{10}$ 4p levels are very efficiently

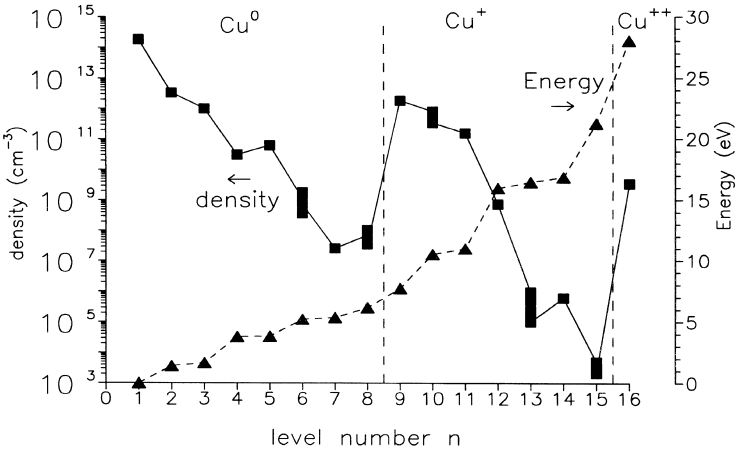

Fig. 8. Level populations at the maximum of their profiles for the various Cu atom and Cu^+ ion levels and for the Cu^{2+} ions (solid line, left axis), as well as their excitation energy (dashed line, right axis).

populated by electron impact excitation from the ground state, whereas the latter process is absent for the $3d^{10}$ 5s level (optically forbidden transition, hence low probability for electron impact excitation).

For the Cu^+ ions, no straight line can be detected, illustrating that the Cu^+ ion excited levels are not Boltzmann distributed. Indeed, the Cu^+ $3d^9$ 4s levels ($E = 10.5$–11 eV) are somewhat overpopulated, since they can be formed by Penning ionization and electron impact ionization, and they cannot decay to the ground state by emission of radiation (metastable levels). Moreover, the Cu^+ $3d^9$ 4p $^3P_2$ level is also clearly overpopulated, due to the very selective asymmetric charge transfer ionization to this level (see above, and see below). Hence, it can be concluded that due to the possibility of Penning ionization and asymmetric charge transfer to some Cu^+ ion levels, and due to the impossibility of radiative decay from the metastable levels, significant deviation from the Boltzmann equilibrium occurs, and hence, the glow discharge is not in local thermodynamic equilibrium (LTE).

3.2. Populating and depopulating processes

Beside the populations of the various levels, the model gives also information about the relative importance of the different populating and depopulating processes taken into account in the model. The relative contributions (in %) of the various processes, integrated over the entire three-dimensional discharge region, are shown in Table 2. It should be mentioned that only those processes for which a contribution $\geq$ 0.1% was calculated, are included in the table, because the other processes can be considered negligible. Moreover, diffusion and/or migration towards the walls (where de-excitation and/or neutralization can occur) can also account for loss of the Cu species. This is, however, not included in the table, because it is difficult to assign a number for it. However, it should be mentioned that this can be an important loss mechanism for all Cu species (except for the Cu atoms in the ground state).

3.2.1. Cu atoms

It appears that the Cu ground state atoms are predominantly populated by sputtering at the cathode, which is the only real source of Cu species in the glow discharge. Depopulation of this level is mainly given by ionization (especially Penning ionization and asymmetric charge transfer) and also by excitation to higher levels (in particular the $3d^{10}$ 4p levels, $n = 4$ and 5, as was expected from the cross section curves in Fig. 2).

Concerning the $3d^9$ $4s^2$ Cu atom metastable levels ($n = 2$ and 3), it follows that the most important production and loss processes are given by electron impact excitation and de-excitation to the other $3d^9$ $4s^2$ level (from 2 to 3 and vice versa). Hence, these levels are strongly coupled to each other, which is not

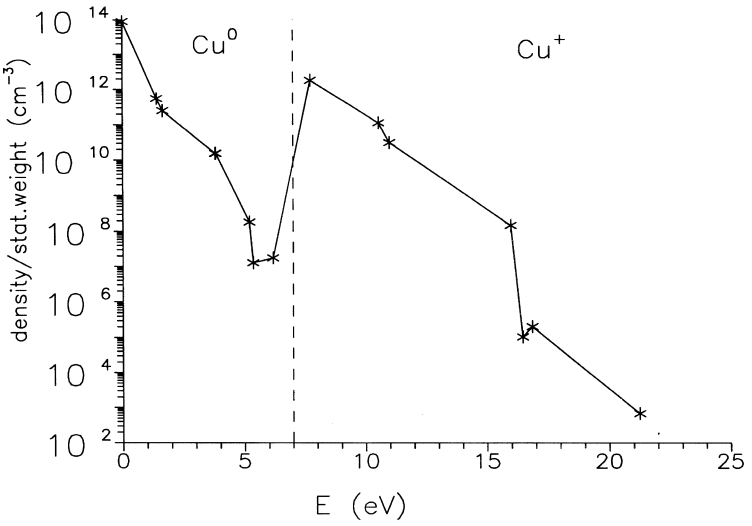

Fig. 9. Level populations at the maximum of their profiles, divided by the statistical weight, for the various Cu atom and Cu^+ ion levels, as a function of their excitation energy.

unexpected, due to the small energy gap (0.253 eV). Beside these coupling processes, the $3d^9\,4s^2$ levels are also populated by electron impact excitation from the Cu atom ground state ($n = 1$) and by radiative decay from the $3d^{10}$ 4p levels ($n = 4$ and 5). Depopulation of these levels occurs also by electron impact de-excitation to the ground state.

The $3d^{10}$ 4p levels ($n = 4$ and 5) are also strongly coupled (the energy gap is even smaller). This strong coupling was already anticipated; therefore, excitation and de-excitation between these levels were not incorporated in the model, because both processes are equally important (due to the small energy gap) and they will not perturb the level populations, the ratio of which is determined only by their statistical weights. Beside this coupling, which is hence not incorporated in the table, the $3d^{10}$ 4p levels are predominantly populated by electron impact excitation from the Cu atom ground state, whereas loss of these levels occurs mainly by radiative decay to the Cu atom ground state ($n = 1$) and to the $3d^9\,4s^2$ metastable levels ($n = 2$ and 3).

A similar story holds for the $3d^9$ 4s 4p quadruplet levels ($n = 6$). The dominant production process is also given by electron impact excitation from the Cu atom ground state ($n = 1$), although electron impact excitation from the $3d^9\,4s^2$ metastable levels ($n = 2$ and 3; stepwise excitation) is not negligible. Moreover, the most significant loss occurs also by radiative decay to the Cu atom ground state and $3d^9\,4s^2$ metastable levels.

For the $3d^{10}$ 5s level ($n = 7$), electron impact excitation from the Cu atom ground state was not incorporated, because the cross section was not available and it is anticipated that this process is of minor importance for an optically forbidden transition. Production of this level is, however, mainly caused by radiative decay (and also electron impact de-excitation) from the $3d^{10}$ 5p levels (belonging to $n = 8$), as well as by electron impact excitation from the $3d^{10}$ 4p levels ($n = 4$ and 5). Radiative decay to these latter levels is the dominant loss mechanism.

The $n = 8$ effective level is again almost exclusively populated by electron impact excitation from the ground state, although electron–Cu^+ ion three-body recombination has also a minor contribution. Depopulation of these levels occurs by radiative decay to lower levels, especially to the $3d^{10}$ 4p levels ($n = 4$ and 5).

3.2.2. Cu^+ ions

The Cu^+ ion ground state ($n = 9$) is mainly created by Penning ionization, and to a lesser extent by electron impact ionization and electron impact de-excitation from the $3d^9$ 4s metastable levels ($n = 10$ and 11). Loss of this level is caused by electron impact excita-

tion to higher levels (especially the $3d^9\ 4p\ ^1P_1$ level, $n = 14$), as well as by electron–ion three body recombination to Cu atoms and electron impact ionization to Cu^{2+} ions.

The $3d^9$ 4s metastable levels ($n = 10$ and 11) are also predominantly formed by Penning ionization, although for level $n = 10$, radiative decay from $n = 12$ is a significant production process as well. Indeed, as appeared from Fig. 8, the $3d^9\ 4p\ ^3P_2$ level ($n = 12$) has a rather high population density, and it decays quite efficiently by emission of radiation to the $3d^9\ 4s\ ^3D_3$ level (the Einstein transition probability is about $3 \times 10^8\ s^{-1}$). This line is indeed found to be particularly intense in glow discharges at the conditions under investigation [19]. Loss of the $3d^9$ 4s levels occurs mainly by electron impact de-excitation to the Cu^+ ion ground state.

As mentioned before, the $3d^9\ 4s\ ^3P_2$ level ($n = 12$) is almost exclusively populated by asymmetric charge transfer, whereas the dominant loss of this level is given by radiative decay to the $3d^9$ 4s metastable levels ($n = 10$ and 11; especially via the 224.7 nm line).

The other $3d^9$ 4p levels are predominantly formed by electron impact excitation from the $3d^9$ 4s metastable levels ($n = 10$ and 11) and also from the Cu^+ ion ground state ($n = 9$). The latter is especially true for the $3d^9\ 4p\ ^1P_1$ level ($n = 14$). Depopulation of these levels is caused by radiative decay to the $3d^9$ 4s levels ($n = 10$ and 11) and, for the $3d^9\ 4p\ ^1P_1$ level, to the Cu^+ ion ground state.

For the $3d^9$ 5s levels ($n = 15$), electron impact excitation from the Cu^+ ion ground state is not incorporated in the model, since the cross section is unknown and it is expected to be quite low anyhow for an optically forbidden transition. The most important production process was found to be electron–Cu^{2+} ion three-body recombination, which is indeed more effective than electron–Cu^+ recombination (see above). Radiative decay to the $3d^9$ 4p levels ($n = 12$, 13 and 14) is the responsible loss mechanism.

3.2.3. Cu^{2+} ions

Finally, the Cu^{2+} ions are formed by electron impact ionization. Although the cross section for double ionization from the Cu atoms is clearly lower than for ionization from the Cu^+ ions, it is still the most significant production process, due to the higher Cu atom density. Nevertheless, ionization from the Cu^+ ion ground state ($n = 9$) and metastable levels ($n = 10$ and 11) play also a non-negligible role. Destruction of the Cu^{2+} ions seems to be solely determined by electron–Cu^{2+} ion three-body recombination, which was the only loss mechanism incorporated in the model.

4. Conclusion

A collisional–radiative model has been developed for the sputtered Cu atoms and corresponding Cu^+ and Cu^{2+} ions in an argon glow discharge, at typical conditions used for GD-OES. The model consists of 8 Cu atom levels, 7 Cu^+ ion levels, and the Cu^{2+} ion species. Electron, Ar and Cu atom impact excitation and de-excitation between the various levels are taken into account, as well as radiative decay between the levels, electron impact ionization and electron–ion three-body recombination. Moreover, Penning ionization with Ar metastable atoms and asymmetric charge transfer with Ar ions are taken into account as additional ionization processes.

The populations of the various levels were calculated in two dimensions (cylindrically symmetrical cell). Both the Cu atoms and Cu^+ ions occur mainly in the ground state, and the level populations of excited levels decreases over many orders of magnitude with increasing excitation energy. The ratio of Cu^+ ion to Cu atom density and of Cu^{2+} ion to Cu^+ ion density were both estimated to be in the order of 10^{-2}.

The relative contributions of the various populating and depopulating processes for all levels were determined. Sputtering from the cathode is the dominant production process for the Cu atoms in the ground state, whereas depopulation is caused by ionization (especially Penning ionization and asymmetric charge transfer) and excitation to Cu atom excited levels. These Cu atom excited levels are mainly formed by electron impact excitation from the Cu atom ground state and by radiative decay from higher excited levels. The latter process (radiative decay to lower levels) is also responsible for the majority of loss from these levels. The Cu^+ ions, both in the ground state and in the $3d^9$ 4s metastable levels are predominantly formed by Penning ionization. Loss of the Cu^+

ion ground state occurs by electron impact excitation to higher levels, as well as by electron impact ionization and electron–ion three-body recombination. The Cu^+ ion metastable levels are mainly depopulated by electron impact de-excitation to the ground state. The Cu^+ $3d^9$ $4p$ $^3P_2$ level is almost exclusively created by asymmetric charge transfer, whereas the other $3d^9$ $4p$ levels are formed by electron impact excitation from the Cu^+ $3d^9$ $4s$ metastable levels and from the Cu^+ ground state. Production of the $3d^9$ $5s$ levels occurs by electron–Cu^{2+} ion three-body recombination. All these Cu^+ ion levels are depopulated by radiative decay to the lower levels. Finally, it was calculated that the Cu^{2+} ions are mainly formed by double electron impact ionization from Cu atoms and that they are lost by electron–ion three-body recombination.

From the above discussion, it follows that radiative decay is the most important loss mechanism for the (non-metastable) excited levels. In a subsequent paper [77], the intensities of the photons emitted by radiative decay will be calculated, and the optical emission spectrum of sputtered Cu atoms and Cu^+ ions will be predicted, which is of direct analytical importance for GD-OES. Moreover, beside the link to GD-OES, this model can also be of interest for plasma diagnostic studies (intensities of spectral lines) and for metal vapor lasers.

Acknowledgements

A. Bogaerts is indebted to the Fund for Scientific Research (FWO), Flanders, for financial support. A. Bogaerts and R. Gijbels also acknowledge financial support from the Federal Services for Scientific, Technical and Cultural Affairs (DWTC/SSTC) of the Prime Minister's Office through IUAP-IV (Conv. P4/10). R. Carman thanks the Australian Research Council for financial support. Finally, we would like to thank Dr. Scheibner and Dr. Griffin, for providing electron impact cross section data for Cu atoms and Cu ions, and also Dr. Vlcek for his interesting discussions about the escape factors.

References

[1] R.K. Marcus, Glow Discharge Spectroscopies, Plenum Press, New York, 1993.
[2] R. Payling, D. Jones, A. Bengtson, Glow Discharge Optical Emission Spectrometry, Wiley, New York, 1997.
[3] A. Bogaerts, M. van Straaten, R. Gijbels, Spectrochim. Acta B 50 (1995) 179.
[4] A. Bogaerts, M. van Straaten, R. Gijbels, J. Appl. Phys. 77 (1995) 1868.
[5] A. Bogaerts, R. Gijbels, W.J. Goedheer, J. Appl. Phys. 78 (1995) 2233.
[6] A. Bogaerts, R. Gijbels, Phys. Rev. A 52 (1995) 3743.
[7] A. Bogaerts, R. Gijbels, J. Appl. Phys. 78 (1995) 6427.
[8] A. Bogaerts, R. Gijbels, J. Appl. Phys. 79 (1996) 1279.
[9] A. Bogaerts, R. Gijbels, W.J. Goedheer, Anal. Chem. 68 (1996) 2296.
[10] A. Bogaerts, R. Gijbels, Anal. Chem. 68 (1996) 2676.
[11] B. van der Sijde, J.J.A.M. van der Mullen, D.C. Schram, Beitr. Plasmaphys. 24 (1984) 447.
[12] J. Vlcek, J. Phys. D 22 (1989) 623.
[13] F. Guimaraes, J. Bretagne, Plasma Sources Sci. Technol. 2 (1993) 127.
[14] A. Bogaerts, R. Gijbels, J. Vlcek, J. Appl. Phys., 84 (1998) 121.
[15] M.J. Kushner, B.E. Warner, J. Appl. Phys. 54 (1983) 2970.
[16] R.J. Carman, D.J.W. Brown, J.A. Piper, IEEE J. Quant. Electron. 30 (1994) 1876.
[17] R.J. Carman, Opt. Lett. 21 (1996) 872.
[18] R.J. Carman, J. Appl. Phys. 82 (1997) 71.
[19] E.B.M. Steers, R.J. Fielding, J. Anal. At. Spectrom. 2 (1987) 239.
[20] N.P. Ferreira, H.G.C. Human, L.R.P. Butler, Spectrochim. Acta B 35 (1980) 287.
[21] A. Bogaerts, R. Gijbels, Spectrochim. Acta B 53 (1998) 437.
[22] C.E. Moore, Atomic Energy Levels, Nat. Stand. Ref. Data Ser. Nat. Bur. Stand. (US) 35, vol. II, Washington, 1971.
[23] D.U. von Rosenberg, Methods for the Numerical Solution of Partial Differential Equations, Elsevier, New York, 1969.
[24] S. Trajmar, W. Williams, S.K. Srivastava, J. Phys. B 10 (1977) 3323.
[25] C. Flynn, Z. Wei, B. Stumpf, Phys. Rev. A 48 (1993) 1239.
[26] M. Ismail, P.J.O. Teubner, J. Phys. B 28 (1995) 4149.
[27] A.W. Pangantiwar, R. Srivastava, J. Phys. B 21 (1988) 2655.
[28] A.Z. Msezane, R.J.W. Henry, Phys. Rev. A 33 (1986) 1631.
[29] K.F. Scheibner, A.U. Hazi, R.J.W. Henry, Phys. Rev. A 35 (1987) 4869.
[30] D.H. Madison, J. Schroeder, K. Bartschat, R.P. McEachran, J. Phys. B 28 (1995) 4841.
[31] K.F. Scheibner, A.U. Hazi, unpublished results.
[32] A. Bielski, J. Quant. Spectrosc. Radiat. Transfer 15 (1975) 463.
[33] M.A. Cayless, Br. J. Appl. Phys. 10 (1959) 186.
[34] D.C. Griffin, M.S. Pindzola, J. Phys. B 28 (1995) 4347.
[35] M.K. Gailitis, Opt. Spectrosc. 14 (1963) 249.
[36] R.S. Freund, R.C. Wetzel, R.J. Shul, T.R. Hayes, Phys. Rev. A 41 (1990) 3575.
[37] W. Lotz, Z. Phys. 232 (1970) 101.
[38] M. Gryzinski, Phys. Rev. A 138 (1965) 336.
[39] R.J. Carman, IEEE J. Quant. Electron. 26 (1990) 1588.

[40] A. Bogaerts, A. Quentmeier, N. Jakubowski, R. Gijels, Spectrochim. Acta B 50 (1995) 1337.
[41] H.-L. Chen, G. Erbert, J. Chem. Phys. 78 (1983) 4985.
[42] L.A. Riseberg, W.F. Parks, L.D. Schearer, Phys. Rev. A 8 (1973) 1962.
[43] S. Inaba, T. Goto, S. Hattori, J. Phys. Soc. Jpn. 52 (1983) 1164.
[44] A. Ben-Amar, R. Shuker, G. Erez, E. Miron, Appl. Phys. Lett. 38 (1981) 763.
[45] S. Inaba, T. Goto, S. Hattori, J. Phys. B 14 (1981) 507.
[46] S. Inaba, T. Goto, S. Hattori, J. Chem. Phys. 75 (1981) 5209.
[47] S. Inaba, T. Goto, S. Hattori, J. Phys. Soc. Jpn. 51 (1981) 627.
[48] S. Inaba, T. Goto, S. Hattori, J. Phys. D 15 (1982) 35.
[49] P. Baltayan, J.C. Pebay-Peyroula, N. Sadeghi, J. Phys. B 19 (1986) 2695.
[50] P. Baltayan, J.C. Pebay-Peyroula, N. Sadeghi, J. Phys. B 18 (1985) 3618.
[51] V.A. Kartazaev, Y.A. Tolmachev, Opt. Spectrosc. 45 (1979) 620.
[52] O.P. Bochkova, I.A. Ivakin, A.V. Kuligin, V.N. Ostrovskii, Y.A. Tolmachev, Opt. Spectrosc. 70 (1991) 9.
[53] A.R. Turner-Smith, J.M. Green, C.E. Webb, J. Phys. B 6 (1973) 114.
[54] R. Johnsen, M.A. Biondi, J. Chem. Phys. 73 (1980) 5045.
[55] V.N. Ostrovskii, Sov. Phys. JETP 57 (1983) 766.
[56] A.K. Belyaev, J. Phys. B 26 (1993) 3877.
[57] R. Johnsen, M.T. Leu, M.A. Biondi, Phys. Rev. A 8 (1973) 1808.
[58] M.S. Aleksandrov, O.P. Bochkova, V.S. Ivanov, A.V. Kuligin, Y.A. Piotrovskii, Y.A. Tolmachev, Opt. Spectrosc. 69 (1991) 311.
[59] Y.A. Piotrovskii, Y.A. Tolmachev, S.V. Kasyanenko, Opt. Spectrosc. 52 (1982) 452.
[60] H.A. Schuessler, C.H. Holder Jr., O. Chun-Sing, Phys. Rev. A 28 (1983) 1817.
[61] D. Fogel, Y.A. Tolmachev, Opt. Spectrosc. 49 (1980) 450.
[62] V.A. Kartazaev, Y.A. Piotrovskii, Y.A. Tolmachev, Opt. Spectrosc. 44 (1978) 362.
[63] J.M. Green, C.E. Webb, J. Phys. B 7 (1974) 1698.
[64] S.C. Rae, R.C. Tobin, J. Appl. Phys. 64 (1988) 1418.
[65] W.L. Wiese, G.A. Martin, Wavelengths and Transition Probabilities for Atoms and Atomic Ions, Part II: Transition Probabilities, Nat. Bur. Stand. Washington, 1980.
[66] A. Kono, S. Hattori, J. Opt. Soc. Am. 72 (1982) 601.
[67] T. Holstein, Phys. Rev. 83 (1951) 1159.
[68] P.J. Walsh, Phys. Rev. 116 (1959) 511.
[69] J.W. Mills, G.M. Hieftje, Spectrochim. Acta B 39 (1984) 859.
[70] J.O. Hirschfelder, C.F. Curtiss, R.B. Bird, Molecular Theory of Gases and Liquids, John Wiley, New York, 1964.
[71] E.W. McDaniel, Collision Phenomena in Ionized Gases, John Wiley, New York, 1964.
[72] W.W. Harrison, B.L. Bentz, Prog. Analyt. Spectrosc. 11 (1988) 53.
[73] J.A. Valles-Abarca, A. Gras-Marti, J. Appl. Phys. 55 (1984) 1370.
[74] N. Matsunami, Y. Yamamura, Y. Itikawa, N. Itoh, Y. Kazumata, S. Miyagawa, K. Morita, R. Shimizu, H. Tawara, Atom. Data and Nucl. Data Tables 31 (1984) 1.
[75] A. Bogaerts, E. Wagner, B.W. Smith, J.D. Winefordner, D. Pollmann, W.W. Harrison, R. Gijbels, Spectrochim. Acta B 52 (1997) 205.
[76] V. Hoffmann, G. Ehrlich, Spectrochim. Acta B 50 (1995) 607.
[77] A. Bogaerts, R. Gijbels, J. Anal. At. Spectrom. 13 (1998) 721.